UiT The Arctic University of Norway

Faculty of Science and Technology

Underwater Inductive Power Transfer with Wireless Charging Applications

Proposal of a wireless charging system for charging small boats

Lydiah Mitchelle Monari

Master's thesis in Electrical Engineering ELE- 3900 May 2022

ACKNOWLEDGEMENT

Through the writing of this thesis, I have received immense support from countless people. First, I would like to thank my supervisors Bjarte Hoff and Hussein Al-Sallami for offering advice and encouragement with a perfect blend of insight and motivation. I'm proud of and grateful for my time working with Hussein particularly. Thank you for your guidance and constructive feedback. I have benefited greatly from your wealth of knowledge and meticulous editing. I am extremely grateful that you took me on as a student and continued to have faith in me over the months.

Thank you to several other professors in the department who introduced the concepts used in this paper over the years.

I am indebted also to several class members. My sincere thanks to Andreas particularly for helping me find my footing, for your generosity and for the company during the long hours in the lab.

Lastly, I want to thank my family for their encouragement and overwhelming support. You were my source of inspiration, and I would not have finished this without you.

ABSTRACT

Underwater wireless power transfer (UWPT) has become an area of great interest due to the advancement of autonomous underwater vehicles (AUVs) and electic boats. This paper seeks to investigate the variation of the coupling coefficient and power transfer in air versus in seawater.

The design is based on a class E converter as it can achieve soft-switching inherently. I made the transmitter and receiver coils then measured self-inductance and parasitic resistance in air and in water. I noted that self-inductance increases when they are placed in water but the mutual inductance is lower. I then calculated the component values for the class E converter based on inductor values (140 µH and 105 µH) and simulated the circuit on LTspice. The power at the output was 74W which is lower than the required value. However, I noted that reducing the coils inductance values while maintaining the value of the other passive components increased the efficiency and power at the output upto four times (311W). The final value chosen for making the inductors was 115 µH and 75 µH as these values gave the maximum power at the output while achieving ZVS. I then designed the transmitter and receiver circuits on Altium and printed the PCBs. All the components were then soldered onto the board and the tests done.

Table of Contents

Table of tables

Table of Figures

ABBREVIATIONS

WPT- Wireless Power Transfer

UWPT- Underwater Wireless Power Transfer

IPT- Inductive Power Transfer

IRPT- Inductive Resonant Power Transfer

CPT- Capacitive Power Transfer

MPT- Microwave Power Transfer

AUV- Autonomous Underwater Vehicle

IoUT- Internet of Underwater Things

UAV- Unmanned Aerial Vehicles

EM- Electromagnetic

SLIPT- Simultaneous Lightwave and Information Power Transfer

ZVS- Zero Voltage Switching

ZVDS- Zero Voltage Derivative Switching

ESR- Equivalent Series Resistance

CHAPTER 1: INTRODUCTION

Recently, there has been great advancement in technology and there are very many consumer electronics in the market. The operation of these devices depends on batteries which have a limited battery life hence the need to be constantly recharged for continuous operation. Currently, recharging these devices is done by the conventional means of using wired chargers. This limits mobility of the user creates a mess when charging several devices simultaneously and are subject to depreciation. Wireless charging substitutes the traditional powering concept by transmitting the energy in air in an efficient way to power-up the device.

Wireless Power Transfer is the use of electric and magnetic fields to transfer power over different mediums. A WPT system consists of the transmitter side and the receiver side. The system can have one transmitter and one receiver or multiple transmitters can be used to generate the electromagnetic field while multiple receivers are used to extract the power. Wireless power transfer can be categorized according to:

- Technology being used (far field or near field)
- Number of transmitters and receivers (single or multiple)
- Distance between the transmitter and receiver (short range or long range)
- Amount of power transferred (low or high power)
- Medium (air, underground or underwater)

Air is the most common medium that is currently being used but research has recently extended to using water as the medium of propagation for the electromagnetic waves. UWPT is used to charge AUVs and small electric boats that are being used for exploration and data collection in seas and oceans. These small boats have batteries that need to be recharged often. Designing a wireless power transfer system for charging these small boats will be advantageous because it reduces the amount of work and time needed to replace the batteries. Wireless charging is highly desirable due to the various advantages it presents both in air and underwater.

There are different methods currently being used for WPT. This includes:

- Acoustic waves
- Optical waves } Far field technologies
- Microwaves

- Capacitive
- Inductive } Near field technologies
- Resonant

For far-field operation, the distance between the transmitter and the receiver is greater than the wavelength λ. We cannot use far-field WPT to transfer high-power as it poses a danger to humans due to the high frequencies of operation

In near-field operation, the distance between the transmitter and the receiver is much smaller than the wavelength λ. More power can be transferred using these methods.

The block diagram showing the different sections of a WPT system is shown below.

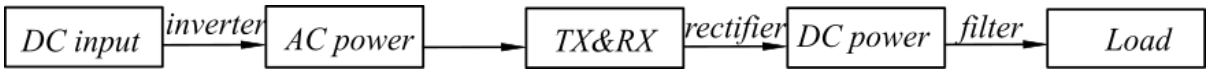

A detailed summary of the WPT system can be found in [1].

1.1 Applications of WPT

Application of WPT can vary from charging mobile devices to the transport industry charging applications. WPT is applied in both low power and high-power applications.

In high power applications, the output power ranges from hundreds of watts to megawatts. The distance between the coils is small and is only a few centimeters apart. High power applications include charging of electric trains [2] where the power output is more than 1MW, electric cars and electric ships.

For low power applications, far field technologies are utilized. The amount of power transferred is very small, but the transfer distance can be large. Low power applications require very little amount of power and include biomedical devices (pacemakers [3] and retinal prostheses [4]), unmanned aerial vehicles (UAV) [5], mobile phone charging [6], smart watches [7] and lamps [8]. IPT is the most used method for charging electric vehicles. Several review papers have been written on the different methods of WPT used for charging electric vehicles including [9] and, [10]. The charging technique could be stationary, dynamic, or quasi stationary/dynamic. The output power is in kilowatts, and the airgap is in few centimeters.

The authors in [11] gives a review of the recent progress of wireless laser power transfer. Also, a summary of the different CPT methods used for various applications ranging from

high power to low power application can be found in [12]. Lastly, a review of microwave power transfer can be found in [13] and [14].

1.2 Research Problem

The research problem for this paper is to analyse UWPT and compare the results with airgap WPT. The analysis will be done in sea water. Water has different electrical properties than air thus posing a challenge when designing a system for UWPT. Some of the factors to consider that are unique to the water environment include: electrical conductivity of water, temperature of water, positional displacement of the coils due to the waves and pressure exerted. However, in this paper, I will study the IPT system under static seawater for simplicity

When designing UWPT system, it is important to specify whether the application will be in fresh water or in sea water as the 2 mediums have different electrical properties as summarized in table 1.

1.3 Research Objectives

The research objectives for this thesis are:

- Investigate the coupling under fresh- and seawater and compare the results with air-gapped system.
- Design a compensation circuit for the system.
- Simulate the system using LTspice software.
- Verify the simulation results by building an experimental setup and test the system in the lab.
- Compare the results underwater and air gapped IPT systems.

1.4 Research Limitations

The challenges that were encountered while working on this thesis include limited time, availability of components and less soldering experience. There was a long delay in delivery of components which had a ripple effect in the project timelines. Thus there was no enough to finish debugging the circuit in the end. I also had very little soldering skills when starting to work on this project. The boards were quite complex hence precision soldering was needed to solder the small components. This took me quite some time to do all the soldering and then fix the mistakes such as short circuits on the tracks and damaged components. Given more time, a lot of the shortcomings in this project would have been solved.

Table 1: Electrical properties of different mediums

Medium	**Relative Permeability**	**Conductivity (S m)**	**Relative Permittivity**
Air	1.00004	0	1.0006
Fresh Water	0.999991	0.01	81
Sea Water	0.999991	4	81

1.5 Thesis Structure

This report is divided into five chapters. Chapter 1 introduced the concept of WPT and the different areas of application. The different technologies used for WPT were briefly mentioned and will be discussed in detail in chapter 2. The research motivation was mentioned, and the research objectives were also listed in this chapter. In chapter 2 we take an in-depth look at the various WPT technologies that are being applied for underwater applications. Chapter 3 will discuss the mathematical models that will be used to design the coils and the class E converter. Experimental and simulation results will be presented in chapter 4. Finally, chapter 5 will give a summary of this work and give suggestions for future work based on the tasks that were not accomplished or any observation that came up while working on this thesis.

CHAPTER 2: LITERATURE REVIEW

Charging of autonomous underwater vehicles (AUVs) and small electric boats is currently being done manually where the boat must be removed from water and the battery replaced before being put back. This is time consuming and may interfere with air tightness of the small electric boats and AUVs hence the need to build a system that can be used to charge the autonomous boats wirelessly.

UWPT is not a new research area. The first research paper can be traced back to 1994 [15]. Since then, many other researchers have made improvements to the original idea to make it more efficient.

For underwater applications, IPT and IRPT are the most used technologies to charge AUVs and small electric boats [16]. It is also used to power modems and sensors for internet of underwater things (IoUT) [17] and for underwater communication systems. Current research in UWPT focuses on charging AUVs and simultaneous transmission of data and power for sensors. Also, more papers have been written about tests done in sea water compared to fresh water.

The various technologies that are currently being implemented are discussed below. A brief description of far field WPT technologies comes first before going into details for near field WPT.

2.1 Far Field Technologies

2.1.1 Optical Wireless Power transfer

Optical WPT systems rely on electromagnetic waves with very high frequency (THz range) for power transfer. The data is sent by a laser diode and received by a receiver that decodes the transmitted symbols and harvests electrical energy from the optical signal.

The power transmitter and its receiver need to be in the line-of-sight for efficient power transfer as the wave cannot traverse them. If the condition holds, the distance can be up to several kilometres [18]. Optical WPT is preferred because of the high data rate due to high frequency of optical carrier. Thus, it provides high data rates for medium ranges compared to both acoustic and radio frequency communication systems.

Underwater optical wireless communication which has Simultaneous Lightwave Information and Power Transfer (SLIPT) uses light waves to transfer energy and data. The harvested energy is in milliwatts and the data rate in kbps. This is explained in [17] and [19].

However, it suffers from water absorption or scattering caused by suspended particles or due to strong disturbance caused by the sun making it less efficient [20].

2.1.2 Acoustic and RF Power Transfer

Acoustic UWPT makes use of sound waves with frequencies higher than the upper audible limit of human hearing. They are used as primary carrier for underwater wireless communication due to their less absorption and long coverage distance. However, it suffers from inter symbol interference due to delay spread. It is also limited to line-of sight scenarios. [21] and [22].

RF waves in underwater communication displays improvement in data rates as it provides higher bandwidth and faster velocity in underwater environment. However, it requires huge antenna size, large transmitter power in fresh water and suffers from high attenuation in sea water [20].

2.2 Near Field Technologies

2.2.1 Capacitive Power Transfer

CPT is the use of electric fields to transfer power. When two metal plates are placed close enough, they act as a capacitor and can be used as the receiver and transmitter. The current induced in the receiver is proportional to the rate of change of the electric field flux between the plates. CPT is advantageous because it is not affected by interference from metallic objects and the electric field is limited to the area between the plates. For larger WPT systems, the metal plates are cheaper compared to using litz wire for IPT and occupies less space than IPT. In addition, CPT has better lateral tolerance than IPT [6].

A review of the research papers shows that there is lesser research on underwater CPT as compared to underwater IPT/IRPT. CPT has the limitation that it requires very high frequencies (above 500KHz) for operation and the obtained capacitance value is small as demonstrated in [23].

Yang was able to achieve bidirectional flow of power (100 W) using CPT at 150 mm for an efficiency of 80.15% in [24]. In [25], CPT was used in fresh water to transmit 400 W over 20

mm with efficiency of 91.3%. In [26], Yang transferred 100 watts over 400 mm at efficiency 50%. Tamura et al. in [27] achieved 94.5% efficiency transferring 1 kW over 20 mm using CPT.

2.2.2 Inductive Power Transfer (IPT) and Inductive Resonant Power Transfer (IRPT)

IPT is based on Faraday's law and Ampere's law. Ampere's Law states a conductor carrying a time varying current creates a magnetic field around it. The magnetic field created is proportional to the size of that electric current with a constant of proportionality equal to the permeability of free space.

If the time-varying magnetic field cuts another coil, a voltage is induced in its terminals. Faraday's law states that a current will be induced in a conductor which is exposed to a changing magnetic field.

The combination of these two laws explains inductive WPT. IPT systems operate at high frequencies and require large coils for the transmitter and receiver. It is easier to implement and operate but has lower efficiency making it less desirable for UWPT.

IRPT is an improvement of IPT. Additional reactive elements are introduced in the system to make it work at resonance. This is known as compensation. The compensation circuit enables the IPT system to operate at a lower frequency range and requires small coils. The different compensation topologies will be discussed later in this chapter.

This project utilizes IRPT hence it will be discussed in detail. IPT and IRPT are the two most common methods for UWPT among the ones listed above since more power can be transferred over longer distances at higher efficiencies than the other methods. Assorted designs with varying number of transmitters and receivers, number of phases and different shapes have been developed to improve the system performance.

In [28], a three-phase coaxial system consisting of 3 inverters and 3 rectifiers is proposed. The 3 receivers and transmitters are arranged to form a circular pattern and the system achieves efficiency of 92.41% operating at 465KHz and an air gap distance of 21 mm. In [29], Kan et al. improved the previous work to make it more stable against misalignment by modifying the structure to have three transmitters and only 1 receiver that is composed of 2 cores. The

efficiency was 86.19% for a maximum power transfer of 745 W. Both are three phase systems.

Assorted designs make use of varying number of transmitters and receivers to increase the efficiency of the system. The proposed system in [30] uses 2 transmitter coils on opposite sides of 1 receiver coil. The system can deliver a maximum power of 300W at efficiency of 85% at 100 mm. In [31], Yan et al. develop a model with one transmitter and 2 double layer receivers which is stable against coil misalignment delivering a maximum power of 664W at efficiency of 92.21%. In [32], the proposed design uses a multiload system that consists of one transmitter and several receivers around the circular transmitter that can be used to charge multiple loads. The system can transfer 500W at efficiency of 90%.

Various shapes for the transmitter and the receiver have also been proposed to increase the efficiency of the system and make the system stable against any misalignment. In [33], Cai et al. design a system where the transmitter and receiver are circumferentially coupled to transmit 630W over 30 mm at efficiency of 89.7%. Wang et al. in [34] develop a novel arc-shaped coupler for UWPT that can transmit 3KW over an air gap of 40 mm at an efficiency of 91.9%. Zeng et al., in [35] used conical and planar spiral coils that makes the system insensitive to misalignment and achieved a efficiency of 83.5% at 30 mm transferring 89.4W. Zhou et al. in [36] proposed a magnetic core structure that improves the coupling while resisting ocean current disturbance. They were able to achieve 92% efficiency when transmitting 3KW over 5mm at a frequency of 35.4KHz.

In all these methods, the power transfer distance varies between 20 mm to 400 mm. Only Hasaba et al. in [37] was able to achieve transmission distance of 10 m by using 7 transmitter coils of diameter 3.4 m located 1.7 m apart.

2.2.3 Eddy Current Losses

The high conductivity of seawater results in eddy current loss in the medium which reduces the efficiency of the system. Therefore, it is necessary to consider all the effects of underwater environment on the UWPT system. Eddy current loss in the seawater increases with the increase in resonant frequency hence very high frequencies should be avoided. The optimum operating frequency of a WPT system in the seawater should be larger than the resonant frequency to achieve the maximum dc–dc efficiency [41]. Kim et al. in [42] developed an impedance model that can be used to make equivalent circuit of the UWPT using Z-parameters. The ECL can be predicted accurately by using the proposed equivalent circuit.

ECL can be simply thought of as the difference between the total loss in sea water and the loss in air.

$$P_{\text{eddy}} = P_{\text{loss}_{\text{seawater}}} - P_{\text{air}} \tag{3.3}$$

Thus, ECL can be modelled as a resistor in the circuit. More analysis of ECL and detuning in sea water using Maxwell's equations can be found in [43].

2.3 Compensation

The main functionality of the compensation network is to resonate with its associated coil so that the reactive power supply is minimized. Compensation networks are designed to improve both the efficiency and the power transfer capability [18]. Some compensation topologies make the system behave as a constant voltage (CV) source or a constant current (CC) source hence eliminating the need for a control system. The efficiency is improved because the reactive impedance (reactance) is zero hence no reactive losses.

Compensation network can be mono-resonant or multi-resonant. Mono-resonant compensation resonates at one frequency and has only one reactive element (capacitor). The topology name corresponds with the location of the capacitor with reference to the inductor. The different mono-resonant compensation topologies are: Series-Series (S-S), Series-Parallel (S-P), Parallel-Series (P-S) and Parallel-Parallel (P-P). The secondary capacitor determines the behaviour of the system. If it is connected in series, the system acts as a voltage source. When connected in parallel, the system can be represented as a current source.

S-S compensation is the most common topology being used because of the ease of application and the choice of primary capacitor does not depend on the load or coupling coefficient. S-S has the advantage that the secondary and primary compensation can be adjusted independently, and it has a high tolerance to misalignment. The value of the resonant inductor and capacitor can be expressed as:

$$w_0 = \frac{1}{\sqrt{L_1 C_1}} = \frac{1}{\sqrt{L_2 C_2}} \tag{2.1}$$

The induced voltage in the secondary due to the primary current I_p is equal to $jwMI_P$, while the reflected voltage in the primary due to the secondary current I_S is equal to $-jwMI_S$, where

M is the mutual inductance between the primary and secondary and ω the operational frequency [38].

Multi-resonant compensation has more reactive elements and it can be LCL or LCC topology. LCC is also commonly applied in advanced syatems because its' efficiency is constant over a greater range of misalignment in both axes. S-S topology has a higher efficiency than LCC due to lower voltage drop by the few components, but LCC requires lower currents in circulation thus requires conductors with smaller cross-section area making it cheaper.

In this project S-S compensation will be utilized. A detailed discussion of the compensation techniques can be found in [39] and [40].

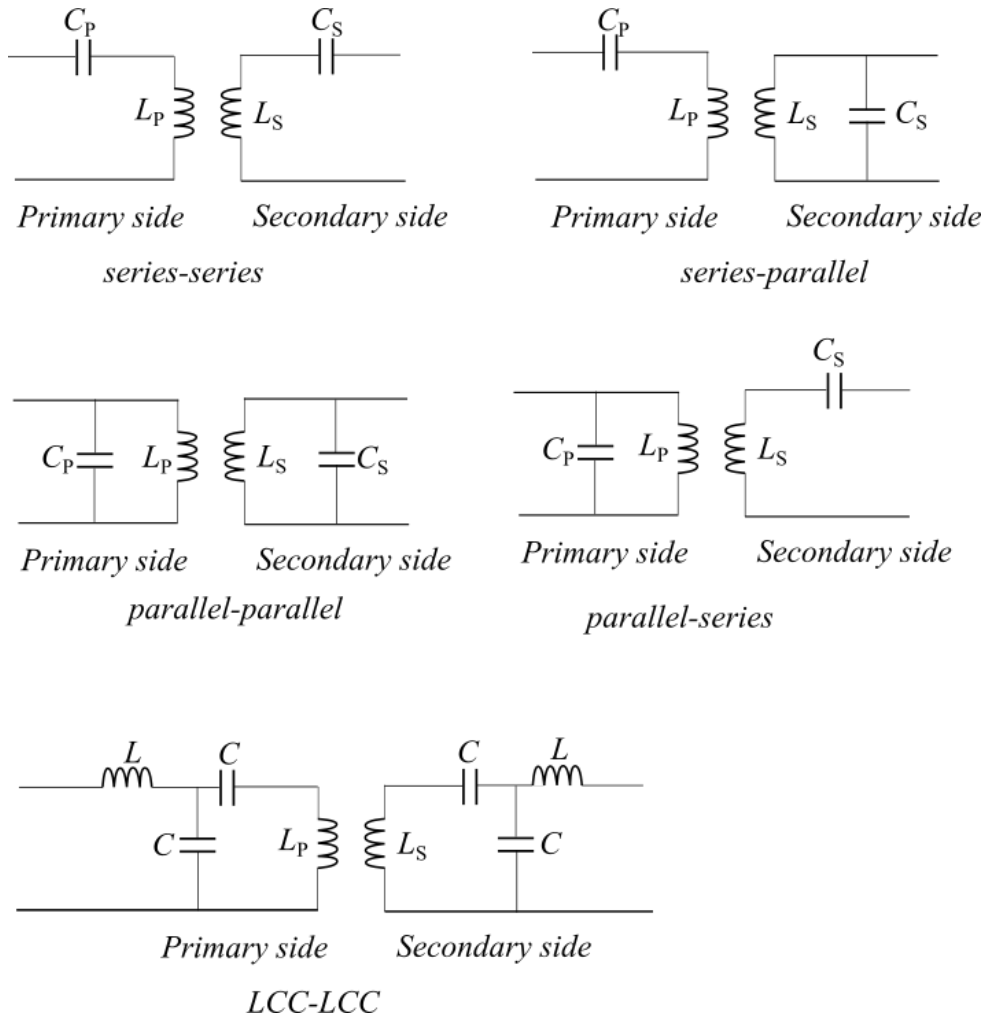

Figure 1: Compensation Topologies

Table 2: Summary of UWPT technologies in the literature

Technology	**Range**	**Directivity**	**Frequency**	**Antenna**	**Applications**	**Papers**
IRPT	Short	Low	kHz – MHz	Transmitter and receiver coils	Charging AUVs	[16], [28], [30], [33], [34], [35], [36], [37]
CPT	Short	Low	kHz – MHz	Metal plate electrodes	Charging AUVs	[23], [24], [25], [26], [27]
Microwaves and Acoustic	Long	High	GHz	Parabolic dishes, rectennas	Communication (IoUT) and powering sensors.	[20]
SLIPT	Long	High	≥THz	Lasers, lenses, fibre optic	Communication and powering sensors	[17], [20], [19], [21]

A summary of the different UWPT technologies is given in the table 2. A detailed review of the different UWPT technologies can be found in [16].

CHAPTER 3: MATHEMATICAL MODELLING

In designing the UWPT system, the two most important sections are the design of the Class E converter and the coil design.

IRPT system is a loosely coupled system because of the low coupling coefficient. Thus, a class-E power amplifier is the most used inverter for WPT [44], [45]. It was first proposed by Sokal and Sokal in 1975 [46]. Since then, scientists have made several adjustments to make it more efficient. There are several topologies of the class-E amplifier, including the traditional model, push-pull configuration, and transformer topology. This paper makes use of the transformer topology. The transformer model is very advantageous, and we can use it for IPT modelling [47].

Class E dc-ac inverter supplies the transmitter coil with ac power that will be transferred to the secondary coil via varying magnetic fields. A Class E inverter is chosen because of the high efficiency due to its low switching losses. The transistor works as a switch and turns on when the voltage is zero hence the name class E zero voltage switching (ZVS) power amplifier. The switch turns on when the voltage across it is zero thus achieving zero voltage switching [48].

A time varying current in the primary winding produces a changing magnetic flux which links with the secondary coil thus inducing a voltage in it. Likewise, the induced voltage in the secondary winding generates a time varying flux that links up with the primary winding. However, not all the flux generated by the two windings links up with the opposite winding. The flux that links up the two windings is known as mutual flux while the flux that gets lost is known as leakage flux. The leakage flux should be minimized to ensure as much of the generated flux reaches the other side. This is the basis of power transfer between the coils [49].

The secondary side consists of a diode rectifier and a L_F-C_F low pass filter. The optimal load resistance to give the desired power is also determined from calculation. The power needs to be rectified and smoothed on the receiver side before being applied to the load, and hence we can use a class-D or class-E rectifier [50]. For this paper, a class E rectifier is used.

3.1 Class E converter

A class E converter consists of a power MOSFET operating as a switch, LCR series-resonant circuit, shunt capacitor C_1, and choke inductor L_F. The switch turns on and off at the chosen operating frequency determined by a driver. The output capacitance of the transistor, the parasitic capacitance of the choke, and stray capacitances are included in the shunt capacitance C_1. The resistor R acts as an ac load. The choke inductance L_F is assumed to be high enough so that the ac current ripple on the dc supply current can be neglected. L, C, and R form a resonant circuit when the switch is on because the capacitance C_1 is short-circuited by the switch. The resonant circuit consists of C_1, L, C, and R connected in series when the switch is off.

Class E power amplifiers are typically used for high frequency applications such as WPT. They can also be scaled up for high frequency high power operations. In calculating the values for the different components, the required input information needed include input DC voltage, required output power, duty ratio and operating frequency.

The design procedure described in [51] was used to design the converter.

Design of Class E converter

Based on the required output power and the given input information such as input DC voltage, duty ratio, coil inductance and operating frequency, we calculate the values for the different components. The following assumptions are made [52]:

- transistor is lossless,
- shunt capacitance is linear,
- RF choke is big enough and allows only dc current,
- there are no losses in the circuit except in the load, and
- a 50% duty ratio

The equations are adapted from [51].

Load resistance at the secondary of the transformer

$$R_{ir} = 0.5768 * \frac{{V_{in}}^2}{P_O} \tag{3.1}$$

Equivalent load resistance referred to the primary side

$$R_i = n^2 * R_{ir} \tag{3.2}$$

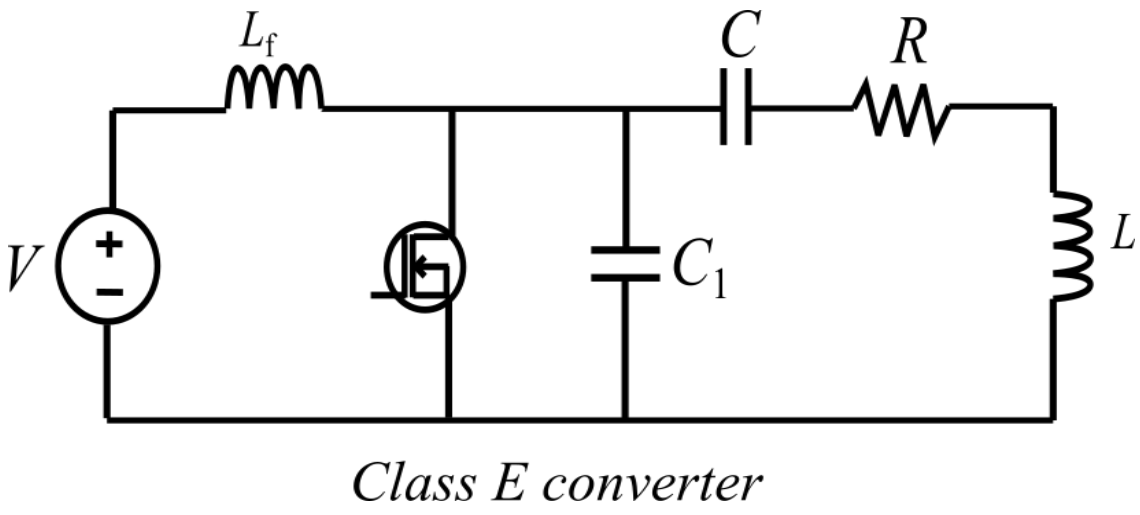

Figure 2: Class E ZVS power amplifier

equivalent input resistance

$$R_{ti} = \frac{w^2 {L_P}^2 k^2 R_i}{{R_i}^2 + w^2 k^2 {L_P}^2} \tag{3.3}$$

equivalent input inductance

$$L_{ti} = \frac{w^2 k^2 L_P^3 (1-k) + L_P R_i^2}{R_i^2 + w^2 k^2 L_P^2} \tag{3.4}$$

magnetizing inductance

$$L_m = \frac{R_i}{w\sqrt{\frac{R_i}{R_{ti}} - 1}} \tag{3.5}$$

primary and secondary leakage inductance

$$L_{ls} = L_{lp} = (1-k) * L_P \tag{3.6}$$

secondary side resonant tank capacitance required to nullify leakage inductance

$$C_S = \frac{n^2}{4\pi^2 f_s^2 (1-k) L_P} \tag{3.7}$$

External inductance

$$L_i = \frac{R_{ti}}{w} Q - \sqrt{\frac{R_i}{R_{ti}} - 1}$$

$$L_{ext} = \mathrm{L}_i - \mathrm{L}_{lp} \tag{3.8}$$

Total inductance in resonant circuit, L

$$L = L_{ext} + \mathrm{L}_{ti} \tag{3.9}$$

Resonant capacitor in series with L

$$C = \frac{1}{w * \left(Q - \frac{\pi(\pi^2 - 4)}{16}\right) * R_{ti}} \quad (3.10)$$

Choke inductance L_F

$$L_F = 6.9348 * \frac{R_{ti}}{4f_s} \quad (3.11)$$

Shunt capacitor

$$C_1 = \frac{8}{w\pi * (\pi^2 + 4) * R_{ti}} \quad (3.12)$$

Output capacitance of mosfet (calculated from datasheet of C3M0075120K mosfet)

$$C_O = C_{OSS} - C_{RSS} \quad (3.13)$$

Actual shunt capacitor value needed

$$C_{1ext} = C_1 - C_O \quad (3.14)$$

3.2 Coil Design

The number of turns needed to give the desired coil inductance is calculated using a combination of Wheeler's formula (below) and the software, **Coil 64**. The coils' shape is chosen to be square.

$$L = \frac{N^2 \times r^2}{8r + 11c} \quad (3.15)$$

Where:

L= required inductance

N= number of turns

r= radius of the coil

c= width of the turns

The software was helpful in giving an approximation of the number of turns needed for the inductor. Wheeler's formula is the underlying principle used in the software. Coil 64 gives values for a circular coil since it is the default shape. I then used Wheeler's formula to fine-tune the calculated number of turns to give the correct value for the square shape.

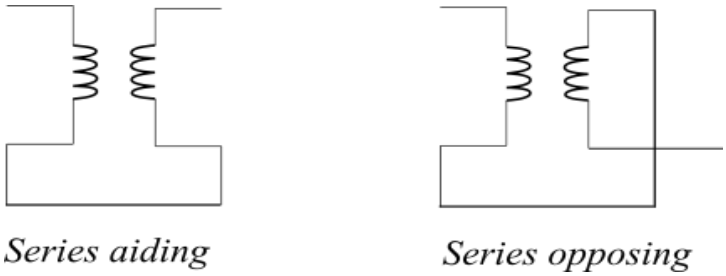

Figure 3: Mutual inductance calculation

Mutual Inductance

Mutual inductance is measured by connecting the coils in series-aiding and then in series-opposing. The difference between the two values divided by four gives the mutual inductance between the coils.

Series aiding

$$L_{aiding} = L_1 + L_2 + 2M \tag{3.16}$$

Series opposing

$$L_{opposing} = L_1 + L_2 - 2M \tag{3.17}$$

Mutual Inductance

$$L_{aiding} - L_{opposing} = 4M \tag{3.18}$$

$$M = \frac{1}{4}(L_{aiding} - L_{opposing})$$

Coupling coefficient (k)

The coupling coefficient shows how strong the primary and secondary coils are linked together by the magnetic fields. The coupling factor is a dimensionless value that defines interaction between the primary and secondary coils of any wireless power transfer system. A higher coupling factor means a more efficient power transfer through reduced magnetic flux loss and less heating. Coupling coefficient varies between 0 and 1; 1 being a perfectly coupled system (no leakage flux). A system could either be tightly or loosely coupled.

The higher the value of k, the more tightly the system is coupled and the higher the efficiency of the system since more power is transferred to the secondary side.

$$k = \frac{M}{\sqrt{L_1 L_2}} \tag{3.19}$$

When k=1 (no leakage inductance),

$$M = \sqrt{L_1 L_2} \quad (H) \tag{3.20}$$

In a real transformer (with leakage inductance),

$$M = k\sqrt{L_1 L_2} \quad (H) \tag{3.21}$$

The leakage inductance of the primary winding is given as

$$L_{l1} = (1 - k_1) \tag{3.22}$$

The leakage inductance of the secondary winding is given as

$$L_{l2} = (1 - k_2) L_2 \tag{3.23}$$

The leakage coefficient h is defined as

$$h = 1 - k = 1 - \frac{M}{\sqrt{L_1 L_2}} \tag{3.24}$$

To reduce the leakage inductances, the windings should be wide and have a low thickness, the insulation between windings should be reduced, one winding should be placed over the other with good overlapping, bifilar windings should be used, and the number of turns should be reduced. Wide and flat windings with a minimum isolation reduce the leakage inductance [49].

The transformer circuit diagram can be simplified to an equivalent T circuit as shown in figure 4.

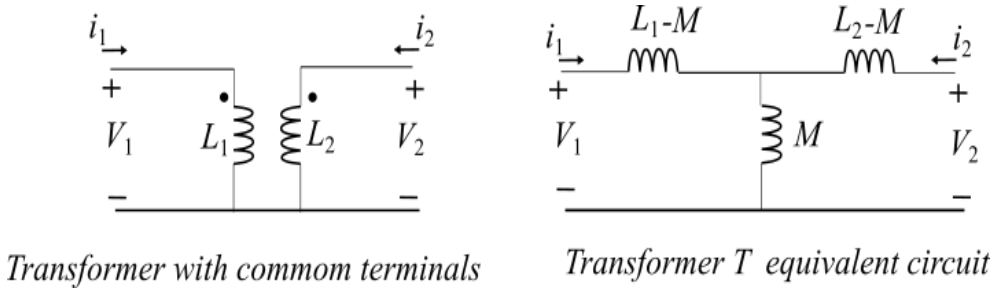

Figure 4: Noninverting transformer T model

The power transfer capability of the system is given by the equation below. Power transfer capability is directly proportional to the mutual inductance (M), input voltage V_{IN} and output voltage V_{OUT}, and is inversely proportional to the frequency of the system ω, and the inductance of compensating coil.

$$P = \frac{M}{\omega L_P L_S} V_{IN} V_{OUT} \tag{3.25}$$

Rectifier

I implemented a class E rectifier so that the system becomes Class E^2. Any other rectifier could be used such as Class D rectifier or a full bridge rectifier. The main components in the rectifier are the diode, the capacitor connected in parallel to the diode, the filter inductor, and the filter capacitor.

The equations for calculating the component values are adopted from [50].

The value of the capacitor parallel to the diode can be calculated using the formula below.

$$C = \frac{C_f}{w^2 L_f C_f - 1} \tag{3.26}$$

The minimum filter inductance that limits the current ripple at the output current is expressed as

$$L_f > \frac{(1 - D)V_O}{0.1 f I_O} \tag{3.27}$$

The minimum filter capacitance is obtained as

$$C_f > \frac{25}{\pi^2 f^2 L_{f_{min}}} \tag{3.28}$$

Chapter summary

The coupling coefficient and mutual inductance between the coils are very important in describing the performance of the circuit. The higher the coupling factor the better the performance of the circuit as more power will be transferred between the coils.

In most cases, the calculated optimum value of the load resistor does not match the standard load resistance. There is need for impedance matching for maximum power transfer to the load at the resonant frequency. Matching circuits are also used to make the amplifier operate optimally despite variations in load or coupling. There are different impedance matching resonant circuits: a Π1a, Π2a, Π1b, Π2b. Analysis of the transformer topology is like Π2a. The matching resonant circuit provides downward impedance transformation.

The choice of components for the class E power converter is important to ensure ZVS. Equation for calculating each component is presented here and will be used in the next chapter.

CHAPTER 4: EXPERIMENTAL AND SIMULATION RESULTS

The circuit was first simulated on LTspice to determine the appropriate values of the different components and to see how the circuit performs.

The frequency of operation for the system is chosen to be 85KHz. This is adopted from SAE J2954 standard for light duty electric vehicles. The standard gives the frequency range 81-90KHz for this type of application. There is no standard set for underwater wireless power transfer yet. There are other standards for WPT in air such as Qi standard. However, all these standards cannot be applied directly to maritime applications due to the high attenuation that is observed underwater when high frequencies are used.

The power required at the output is 300W. The input was chosen to be a 60V dc source for safety reasons. The duty ratio of the mosfet was chosen to be 0.5.

A SiC (Silicon Carbide) mosfet is used in this project. It has a 4^{th} pin, Kelvin source, which delivers an undisturbed signal to the driver. SiC mosfets have several advantages over normal silicon mosfet such as

- reduced switching losses and overall reduction in energy losses,
- higher switching frequencies which allow for smaller peripheral components,
- Increased critical breakdown strength which means higher voltage rating,
- higher temperature operation,
- lower leakage current at higher temperatures

A 4-pin package has a separate driver source pin and power source pin which minimizes the effect of parasitic inductance. This makes it possible to maximize the switching speed of the mosfet due to reduced switching loss across the parasitic inductance. Zikang et. al. in [53] discusses how to utilize SiC devices in high and very high frequency power converters.

4.1 Simulation Results

The circuit design was carried out using equations outlined in chapter 3 and simulated on LTspice. The Matlab script used to do the calculations is copied in the Appendix. Table 3 gives the input specifications required to calculate the component values.

Table 3: Circuit specifications

Input specifications	**Value**
Input voltage	60 V
Operating frequency	85 KHz
Output power	300 W
Duty ratio, D	0.5
Quality factor, Q	7
Primary inductance, L_P	140 µH
Secondary inductance, L_S	105 µH
Coupling coefficient	0.3
Output capacitance (mosfet), C_O	56pF

The inductance of the primary and secondary coil were selected to be 140 µH and 105 µH respectively. The inductor values can be chosen randomly but a higher inductance is preferred because it reduces the amount of current in the circuit. The coupling coefficient between the coils is selected to be 0.3 to emulate the worst-case scenario when the coils are far apart or displaced. The choice of input voltage is also at discretion of the designer even though a higher voltage is preferred for the same reason as the inductors. I chose a duty ratio of 0.5 for simplicity in the calculations. It is the most used value among researchers too.

Table 4: Calculated values

Passive Components	Matched impedance Resonant Circuit
Shunt inductor, L_F	193 µH
Shunt capacitor, C_1	36 nF
Resonant capacitor C	35 nF
External inductor, L_{EXT}	20 µH
Secondary capacitor, C_S	63 nF
Load Resistor, R	7 Ω
Filter inductor (min)	410 µH
Filter capacitor (min)	860 nF
Diode capacitor	6.8nF

Table 4 gives a summary of the output values from the calculation. The overall circuit including the secondary side is shown below.

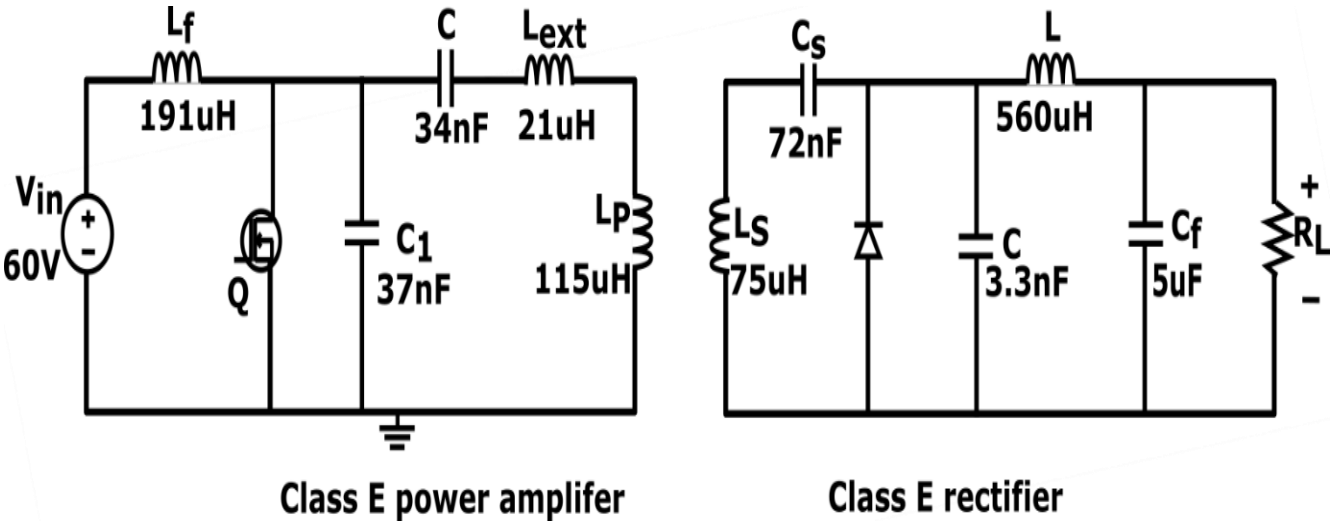

Figure 5:Overall system circuit

Using the calculated values to do a spice simulation, we see that ZVS is maintained and the mosfet losses are low. Using coils 140µH and 105µH and coupling coefficient of 0.3 gives 74W output power and 89.6% efficiency. This is quite low compared to the desired value of 300W. This is attributed to the half bridge rectification that was chosen for this circuit. When simulated using a full bridge rectifier, the output power is 300W. Since I wanted to use a single diode to make the circuit less bulky, there was need to increase the power at the output to a higher value. After several attempts of trying different inductor values, I made an interesting observation. The output power increases as the coil inductances reduces.

Therefore, I maintained the circuit components as they were but reduced the value of the transmitter and receiver coils used for simulation. I observed an increase in the power with the reduction in the value of the coils' inductance.

For instance, when I reduced the inductance of the coils to 130µH and 95µH, the output power increases to 137W with an efficiency of 96.8%. When the inductor was further reduced to 120µH and 85µH, the power at the output increased to 235W with an efficiency of 96.6%. Finally, with 115µH and 75µH, the power at the output increased to 311W, and the efficiency of the system is 97.3%. However, reducing the coils' inductance values to 110µH and 70µH or any value lower than that completely distorts the waveform, and it is no longer sinusoidal and causes very high losses across the MOSFET.

Increasing the coupling coefficient above 0.3 distorts the waveform and there is no ZVS. However, at any coupling coefficient lower than 0.3 the circuit will continue to function with ZVS but the power at the output will be lower. Reducing the load resistor to 5 Ω also increases the power at the output. Based on these results, we can improve the total power transferred and the system efficiency by reducing the inductor values.

Figures 6-9 show the simulated voltage stress over the MOSFET when using different inductor sizes. It is seen from the figures that zero voltage switching (ZVS) is achieved. Furthermore, the body diode conduction losses reduces with increase in the values of the inductances, which explains the improvement in the efficiency.

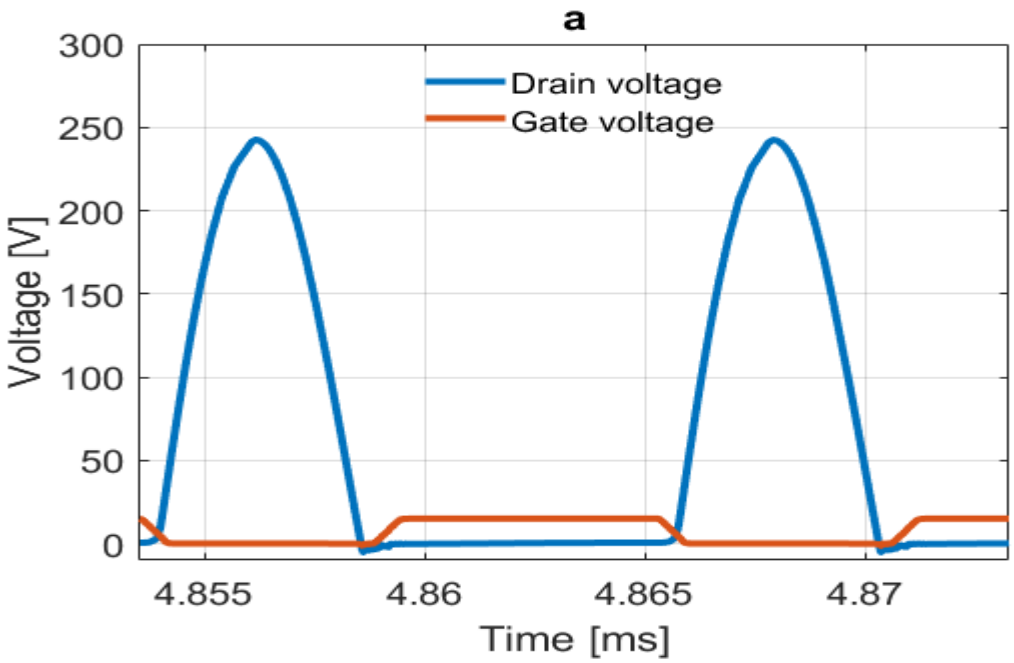

Figure 6: Gate voltage vs drain voltage 140-105uH

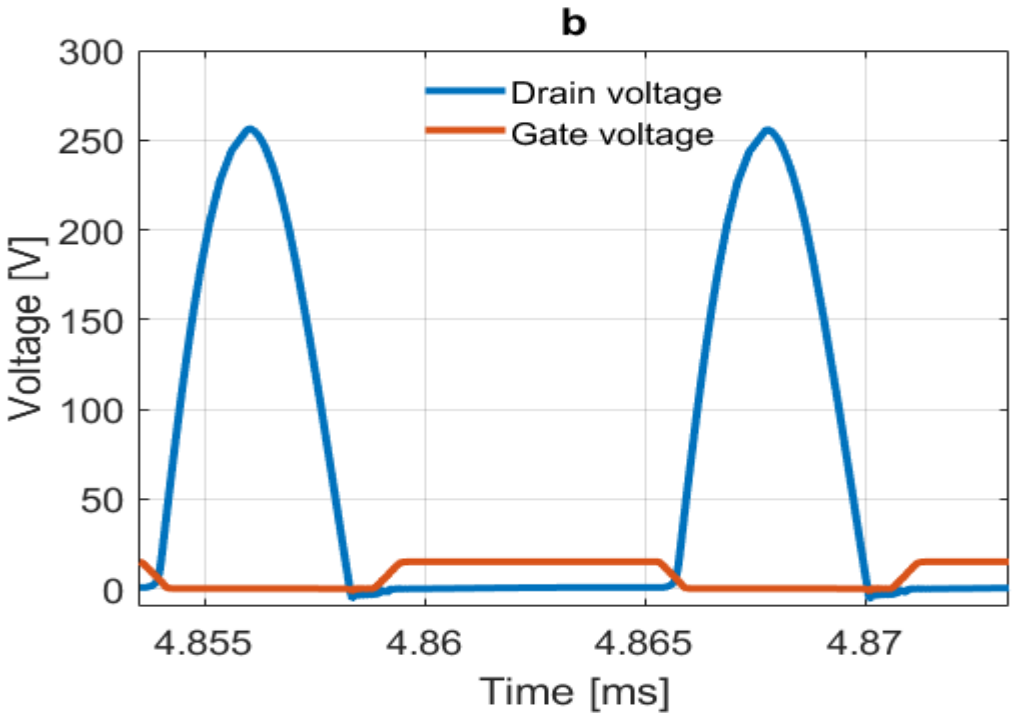

Figure 7: Gate voltage vs drain voltage 130-95uH

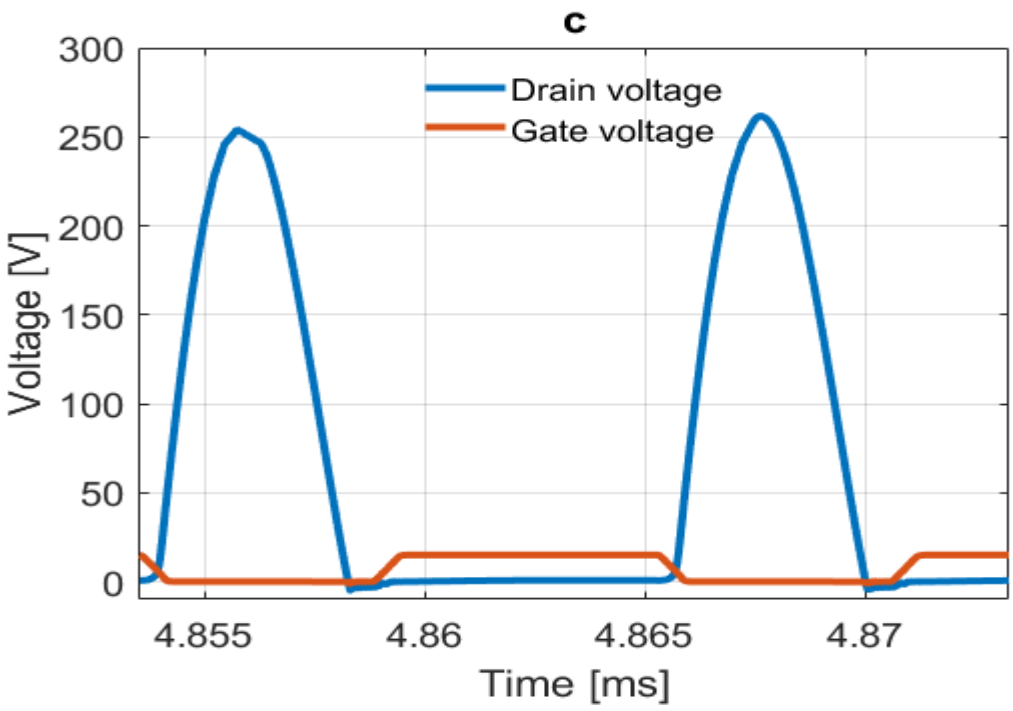

Figure 8: Gate voltage vs drain voltage 120-85uH

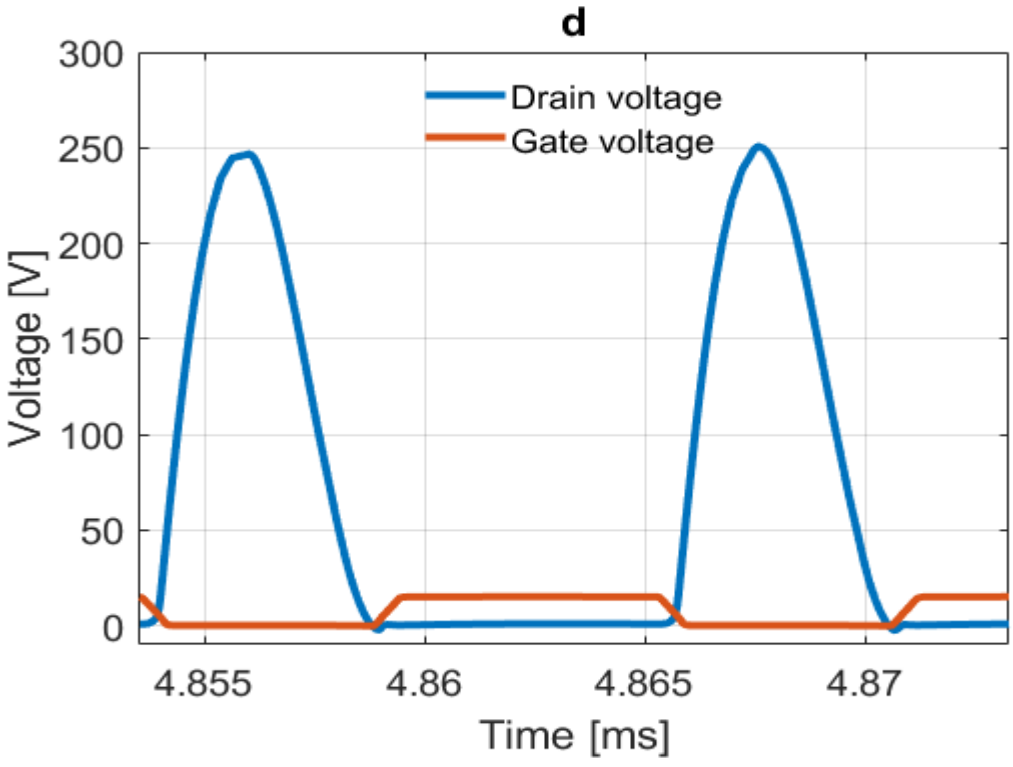

Figure 9: Gate voltage vs drain voltage 110-75uH

In addition, I investigated the transmitter and the receiver coils' current. When the inductance of the coils is decreased, the current across the transmitter and the receiver coils are both increasing as shown in figures 10-13. When the coil inductance is 140µH and 105µH, the maximum receiver current is 4.06A which starts off being less than the maximum transmitter current, which is 5.45A. But with 110µH and 75µH coil inductance, the maximum receiver coil current ends up being almost equal to the transmitter current at 8.6 A and 8.7 A respectively.

Based on the results above, it is possible to have more power at the output without designing a very big coil. With smaller coils, we can have more power and better efficiency at the output while utilizing the same components. The circuit still achieves ZVS.

We can change the shunt capacitor value to adjust the voltage shape across the MOSFET. The input voltage can also be reduced while achieving ZVS. For instance, using 110µH and 75µH for the coils and setting the input voltage to 48V, the output power is 197 W, and the efficiency of the circuit is 96.3%. Nevertheless, the output power is still higher than the original value of designing the circuit.

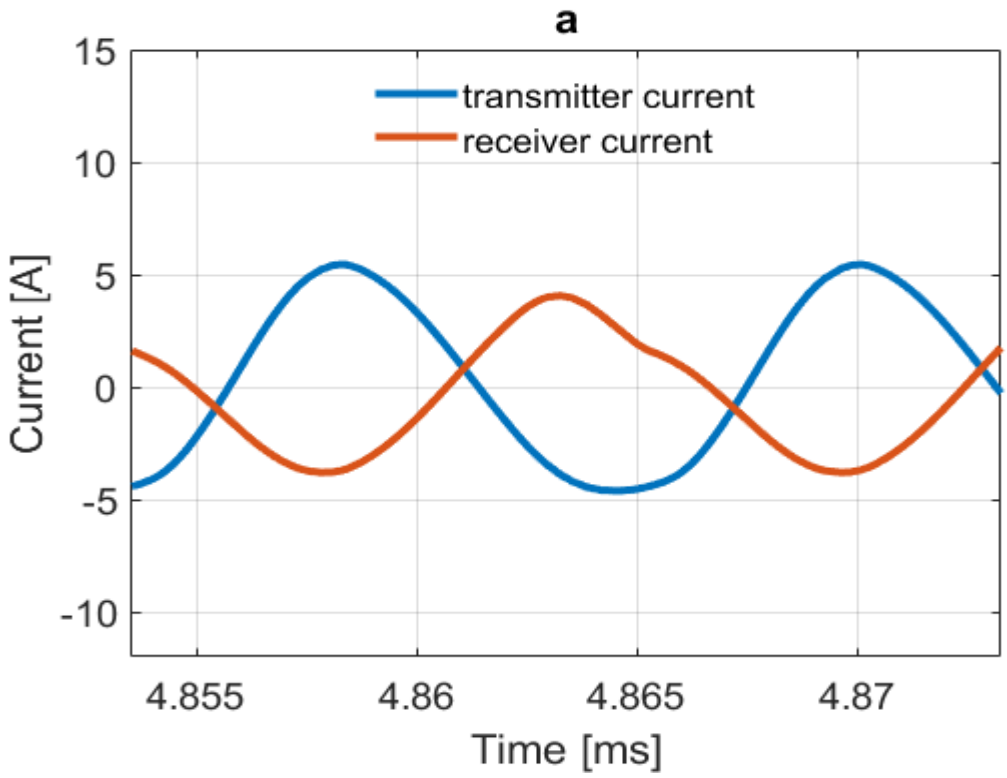

Figure 10: Transmitter current vs receiver current 140-105uH

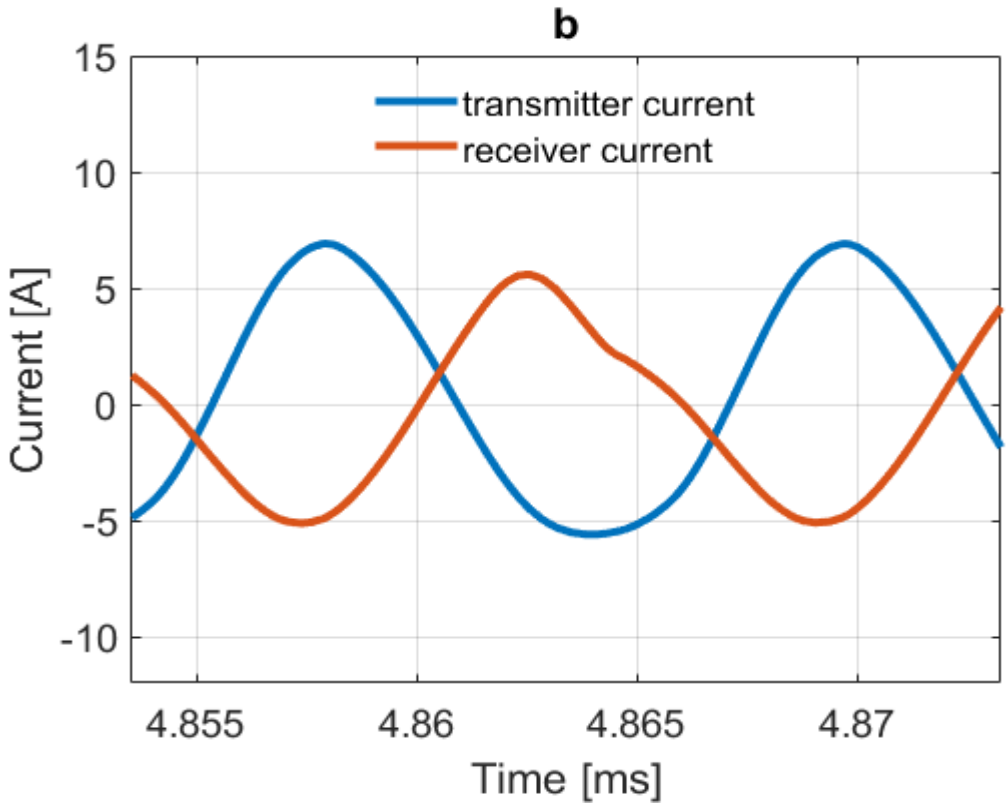

Figure 11: Transmitter current vs receiver current 130-95uH

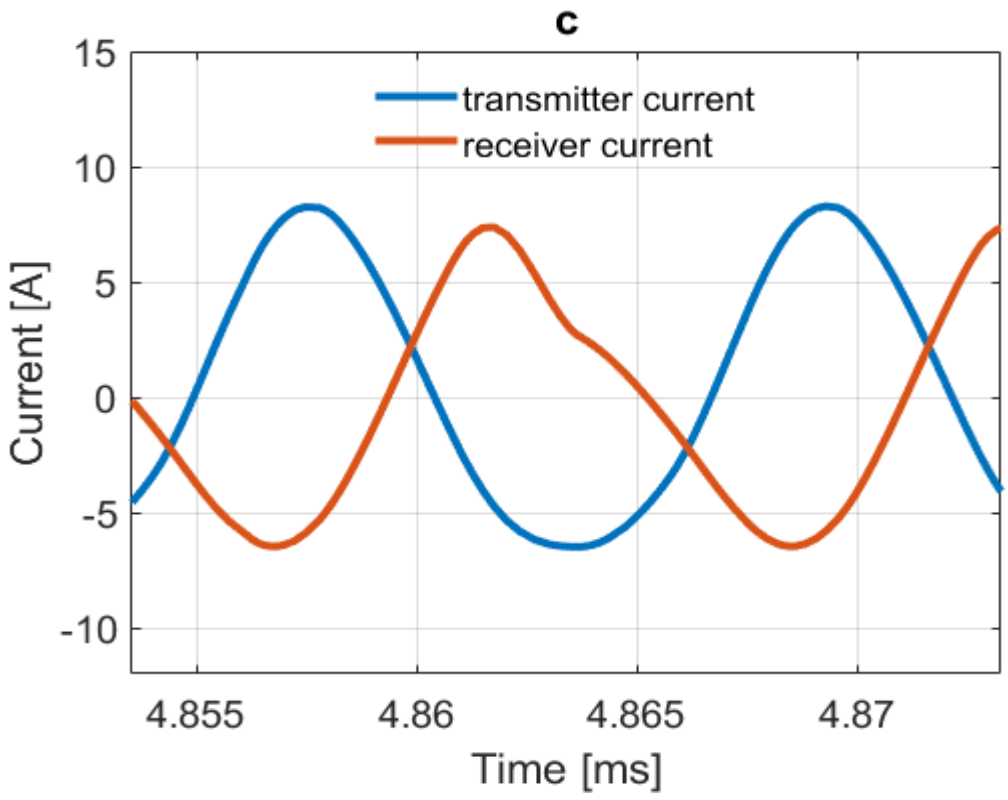

Figure 12: Transmitter current vs receiver current 120-85uH

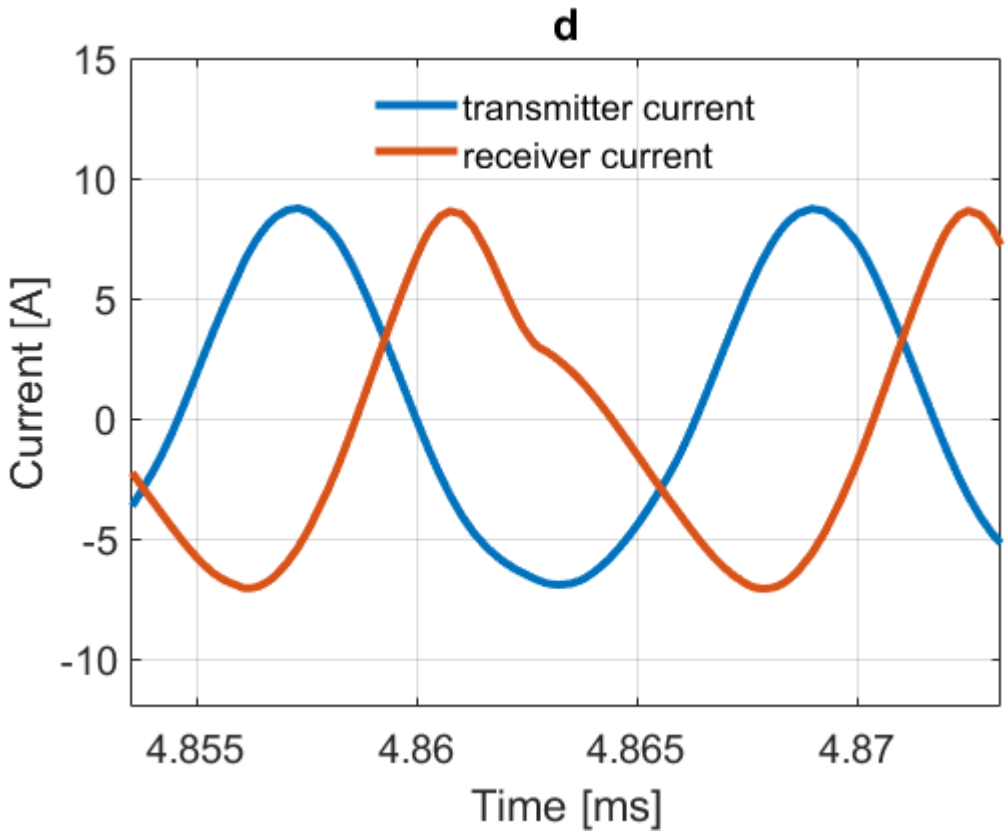

Figure 13: Transmitter current vs receiver current 110-75uH

The Receiver

The receiver is made up of: the secondary coil, a diode rectifier, an L-C low pass filter and the load (resistor). The rectifier can be either full bridge or half bridge. A full bridge rectifier consisting of four diodes which is bulky and not suitable for WPT applications, even though the power at the output is 300W without having to adjust the inductor values.

A Class D or Class E rectifier can be used in this circuit. The difference in the performance of the two configurations is that the voltage stress across the mosfet is higher when using a class D rectifier (290V versus 236V for a class E rectifier). Therefore, the output power is higher when using a class D rectifier. However, for this project, a class E rectifier is chosen so that we have a class E^2 power amplifier circuit. The current in the load is least when using a class E as opposed to any other rectifier configuration.

4.2 Experimental Results

Tests were done in the lab to validate the operation of the circuit. The first tests were on the coils to determine the mutual inductance and the coupling coefficient both in air and underwater. The two circuits (transmitter and receiver) were then designed on Altium and the PCBs printed. Thereafter, all components were soldered onto the boards and the test done in the lab.

All the inductors used in the circuit were made using E-cores. ETD 39 core was used to make the choke inductors while ETD 29 was used to make the external inductor. The number of turns needed to achieve the required inductance was calculated using Coil 64 software. The input choke inductor used is larger than the calculated values as this helps to reduce the transients during turn on of the switch. The calculated value for the choke inductor was 193µH. Very high transcients were observed at turn on while doing the simulation on LTspice. For this reason, I built a 500µH choke inductor as this was observed to lower the transcients significantly.

The electrical properties for un-gapped ETD 39 core are:

A_L= 2800nH $\mu_e \approx$ 1640 airgap≈ 0

B ≥320mT at H = 250 A/m; f = 25 kHz; T = 100 °C

Core loss ≤ 1.4W at f = 100 kHz; B= 100mT; T = 100 °C

Core loss ≤ 2.5W at f = 400 kHz; B= 50mT; T = 100 °C

The electrical properties for un-gapped ETD 29 core are:

A_L= 2200nH $\mu_e \approx$ 1660 airgap≈ 0

B ≥320mT at H = 250 A/m; f = 25 kHz; T = 100 °C

Core loss ≤ 0.65W at f = 100 kHz; B= 100mT; T = 100 °C

Core loss ≤ 1.1W at f = 400 kHz; B= 50mT; T = 100 °C

Where A_L is Inductance factor, B is RMS value of magnetic flux density, H is RMS value of magnetic field strength and μ_e is relative apparent permeability in Vs/Am.

Table 5: Transmitter BOM

Transmitter component list				
	Category	**Design value**	**No.**	**Actual value used**
1	Terminal Blocks	MULTICOMP - MA331-500M03 - TERMINAL BLOCK EUROSTYLE, 3 POSITION, 26-14AWG	1	MULTICOMP - MA331-500M03 - TERMINAL BLOCK EUROSTYLE, 3 POSITION, 26-14AWG
2	RF / Coaxial Connectors	RF SMA Connector, Female, Board Mount, Clamp Solder Terminal, Jack	1	RF SMA Connector, Female, Board Mount, Clamp Solder Terminal, Jack
3	Gate Drivers	Half Bridge Based MOSFET Driver, PDSO16	1	Half Bridge Based MOSFET Driver, PDSO16
4	EMI / RFI Components	FORMER, ETD29, 13PIN	1	FORMER, ETD29, 13PIN
5	Connectors	DC connector. Interconnection Device	6	DC connector. Interconnection Device
6	Chip SMD Resistors	Fixed Resistor, 0.125W, 3900ohm, 150V, 1% +/-Tol, 100ppm/Cel, Surface Mount, 0805	1	Chip-Widerstand, Chip resistor D12, 0805, 5%, E24, 3.9 kΩ
7	Chip SMD Resistors	Fixed Resistor, Thin Film, 0.1W, 15ohm, 100V, 0.1% +/-Tol, 25ppm/Cel, Surface Mount, 0805	1	Chip-Widerstand, Chip resistor D12, 0805, 5%, E24, 15Ω 0805
8	Ceramic Capacitors	0.039 µF ±5% 1000V (1kV) Ceramic Capacitor C0G, NP0 2225 (5763 Metric)	1	Ceramic Capacitor, Multilayer, Ceramic, 1000V, 5% +Tol, 5% -Tol, C0G, 30ppm/Cel TC, 0.033uF, Surface Mount, 2220
9	Ceramic Capacitors	Ceramic Capacitor, Multilayer, Ceramic, 1000V, 5% +Tol, 5% -Tol, C0G, 30ppm/Cel TC, 0.033uF, Surface Mount, 2220	1	Ceramic Capacitor, Multilayer, Ceramic, 1000V, 5% +Tol, 5% -Tol, C0G, 30ppm/Cel TC, 0.033uF, Surface Mount, 2220
10	Ceramic Capacitors	SMD Multilayer Ceramic Capacitor, 22000 pF, 25 V, 0805 [2012 Metric], ± 10%, X7R, WCAP-CSGP	1	SMD Multilayer Ceramic Capacitor, 22000 pF, 25 V, 0805 [2012 Metric], ± 10%, X7R, WCAP-CSGP
11	Ceramic Capacitors	SMD Multilayer Ceramic Capacitor, 68000 pF, 25 V, 0805 [2012 Metric], ± 10%, X7R, WCAP-CSGP	1	0805 PCZ (X7R) / 63V 0.01 µF
12		FERROXCUBE CPH-ETD39-1S-16P-C Transformer Bobbin, 16 Pin, ETD39	1	FERROXCUBE CPH-ETD39-1S-16P-C Transformer Bobbin, 16 Pin, ETD39
14		Power Field-Effect Transistor, 30A I(D), 1200V, 0.09ohm, 1-Element, N-Channel, Silicon Carbide, Metal-oxide Semiconductor FET, TO-247	1	Power Field-Effect Transistor, 30A I(D), 1200V, 0.09ohm, 1-Element, N-Channel, Silicon Carbide, Metal-oxide Semiconductor FET, TO-247

Table 6: Receiver BOM

Receiver component list				
	Category	**Designed component**	**No.**	**Actual component used**
1	Terminal Blocks	MULTICOMP - MA331-500M03 - TERMINAL BLOCK EUROSTYLE, 3 POSITION, 26-14AWG	1	MULTICOMP - MA331-500M03 - TERMINAL BLOCK EUROSTYLE, 3 POSITION, 26-14AWG
2	Ceramic Capacitors	Ceramic Capacitor, Multilayer, Ceramic, 1000V, 10% +Tol, 10% -Tol, X7R, 15% TC, 0.068uF, Surface Mount, 1808	1	Ceramic Capacitor, Multilayer, Ceramic, 1000V, 10% +Tol, 10% -Tol, X7R, 15% TC, 0.068uF, Surface Mount, 1808
3	Ceramic Capacitors	Ceramic Capacitor, Multilayer, Ceramic, 100V, 10% +Tol, 10% -Tol, X7S, 22% TC, 3.3uF, Surface Mount, 1210	1	Ceramic Capacitor, Multilayer, Ceramic, 100V, 10% +Tol, 10% -Tol, X7S, 22% TC, 3.3uF, Surface Mount, 1210
4	Ceramic Capacitors	Ceramic Capacitor, Multilayer, Ceramic, 1000V, 5% +Tol, 5% -Tol, C0G, -/+30ppm/Cel TC, 0.0068uF, Surface Mount, 1210	1	Ceramic Capacitor, Multilayer, Ceramic, 1000V, 5% +Tol, 5% -Tol, C0G, -/+30ppm/Cel TC, 0.0068uF, Surface Mount, 1210
5		Rectifier, Single, 60A, 650V, To-247Ad Rohs Compliant: Yes	1	DIODE SCHOTTKY 600V 4A TO220-F2
6	Uncategorized	Ferrite Accessories Coil Former Black Polyterephthalate	1	Ferrite Accessories Coil Former Black Polyterephthalate
7	Connectors	DC connector. Interconnection Device	2	DC connector. Interconnection Device
9	Chip SMD Resistors	Fixed Resistor, Thin Film, 0.063W, 6.98ohm, 50V, 0.1% +/-Tol, 25ppm/Cel, Surface Mount, 0603	1	Chip-Widerstand, Chip resistor D12, 0805, 5%, E24, 10Ω 0805

Before starting any work in the laboratory, I did a risk assessment to assesss all risks involved when carrying out the experiment. Some of the risks include electric shock and explosion of components. Once the necessary steps to mitigate the risks were put in place, I began doing the tests. I used three power supplies to power different inputs of the transmitter. A function generator was used to provide the 85KHz signal to the gate drive and an oscilloscope used to analyze the waveforms at different points in the circuit.

4.2.1 Coils

Using the software coil 64, the number of turns for the primary coil is 45 while the number of turns in the secondary coil is 37. Substituting the value of L, r, and c in equation (3.15) gives 42 turns for the primary winding and 35 turns for the secondary winding. The results from the software are close to the values calculated using wheeler's formula. Wheeler's formula gives a much better approximation since it considers the shape of the coil. The software, Coil 64, gives results based on a circular coil.

The self-inductance values were measured in the lab using an LCR meter (hp 4285A 75KHz-30MHz Precision LCR Meter). A picture of the test set-up can be seen on the Appendix. The inductance was 116µH for the primary coil and 76µH secondary coil. The primary coil has 42 turns while the secondary coil has 36 turns. The diameter of the coils is 150 mm and 130mm respectively.

The spacing of the wires is assumed to be 1 mm and the wire diameter is 1.12mm. Copper wire of diameter 1.12mm was used for making the coils. Litz wire would have better performance, but it was difficult to work with it because it does not easily take the desired shape, hence the choice to use regular wire.

The coils were then made waterproof by putting them in laminating paper and using a heat gun to seal it completely. Figure 14 shows the shape and the dimension of the coils.

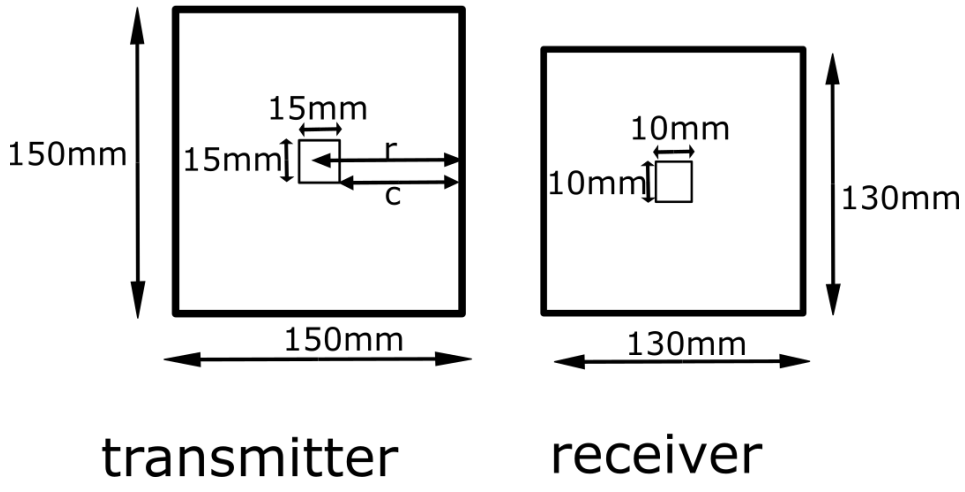

Figure 14: Coil dimensions

For the air-gapped coils, the inductance was 114.21µH for the primary coil and 76.28µH secondary coil. The parasitic resistance for the coils was 0.989Ω and 0.714Ω for the primary and secondary coils, respectively. The maximum mutual inductance is 69.185µH when the

distance is 1cm at which the coupling coefficient is 0.7412. Both the mutual inductance and the coupling factor dramatically decrease with the increase of the distance between the transmitter and the receiver coils, as shown in figure 15.

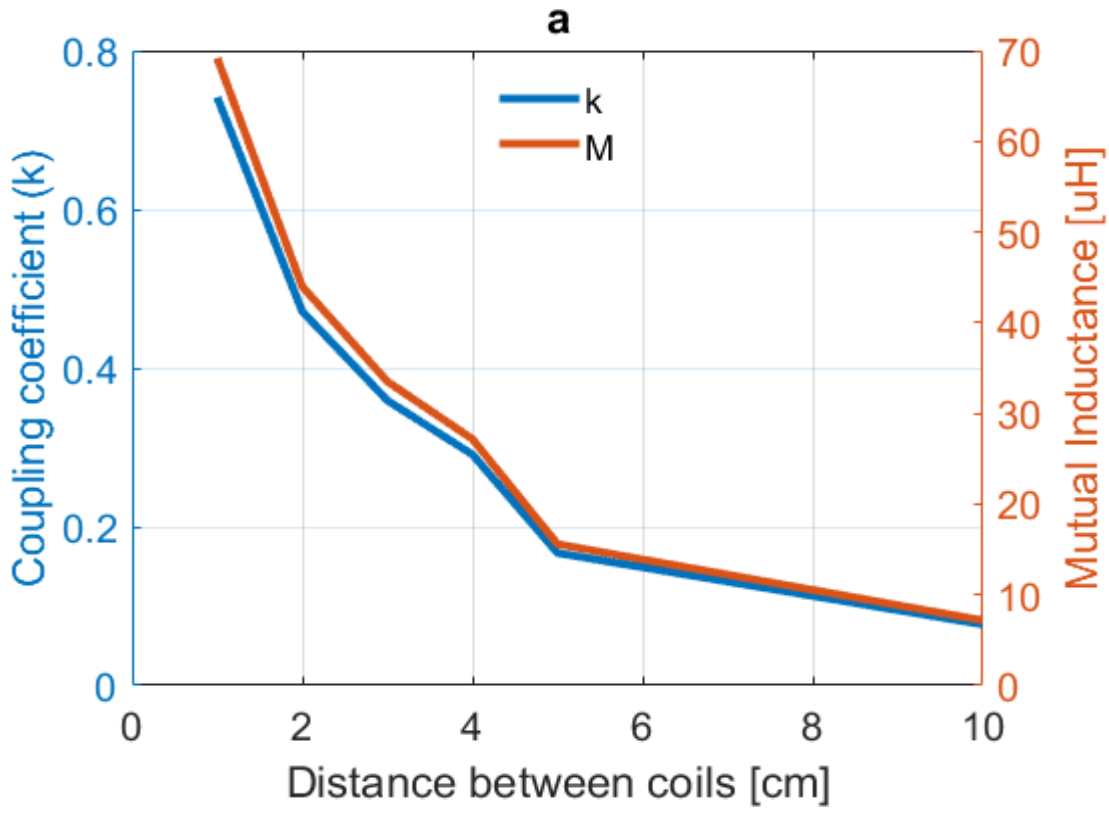

Figure 15: Mutual inductance and coupling coefficient in air

I submerged the coils underwater and took the measurements. The inductance was 116.33µH for the primary coil and 78.28µH secondary coil. The parasitic resistance for the coils was 0.79Ω and 0.56Ω for the primary and secondary coils, respectively. I noticed that the self-inductance of the coils increased when they were submerged underwater while the parasitic resistance decreased. However, the mutual inductance was lower than for the air-gapped coils, which was 57.3µH and with the coupling coefficient was 0.6013. Table 5 lists a comparison between air-gapped coils and coils submerged in the seawater that was collected from a local harbour.

Similar to the results obtained from air-gapped, both the mutual inductance and the coupling factor decreased with the increase of the separation distance between the coils, as shown in figure 16. The curve falls almost linearly when coils are placed underwater but then falls exponentially when the coils are in air. I also noted that self-inductance was slightly increasing in each step as the distance between the coils increased.

Table 7: Coil Parameters underwater and in air

	In Air	Underwater
Primary coil	114.207µH	116.33µH
Secondary coil	76.28µH	78.06µH
Mutual inductance	69.185µH	57.3µH
Coupling coefficient	0.7412	0.6013

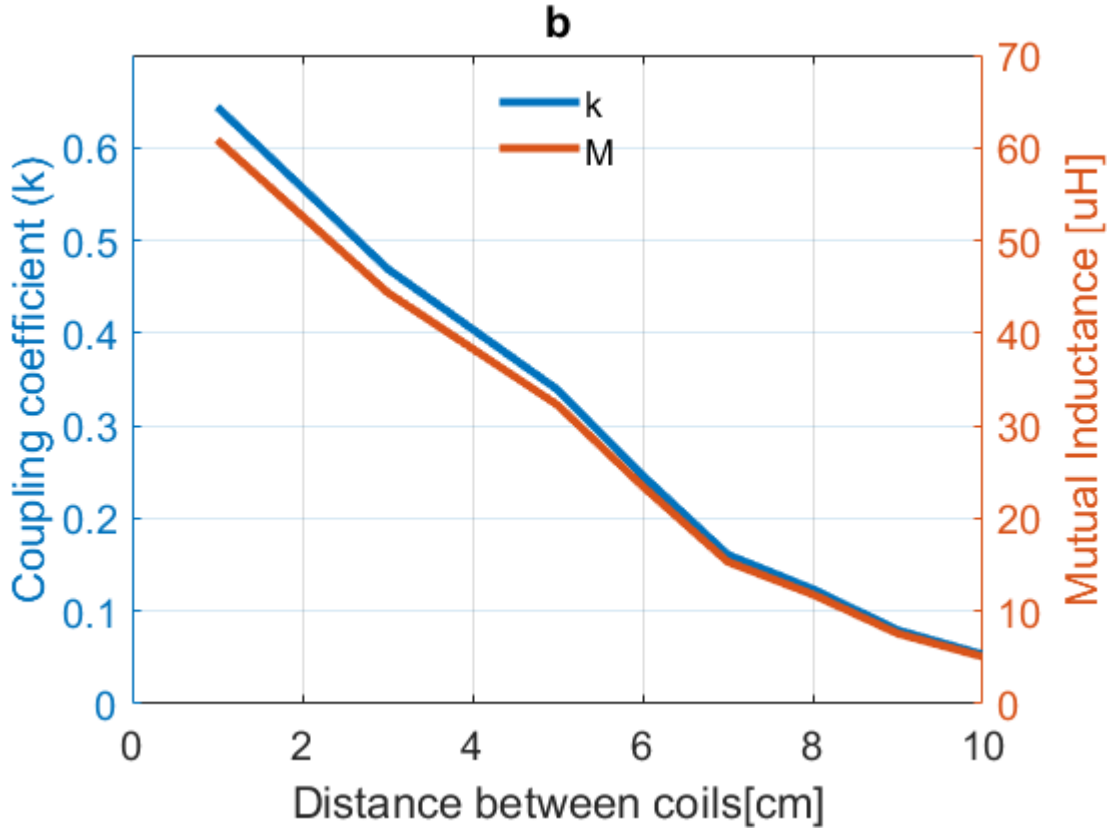

Figure 16: Mutual inductance and coupling coefficient in water

The coupling coefficient and mutual inductance were also measured when the coils were misaligned. First with horizontal misalignment then with vertical misalignment. I observed that mutual inductance and coupling coefficient drop at a higher rate when there is vertical misalignment between the coils than with horizontal misalignment. This can clearly be seen in figures 17-20.

All the results show that mutual inductance in air is higher than in water.

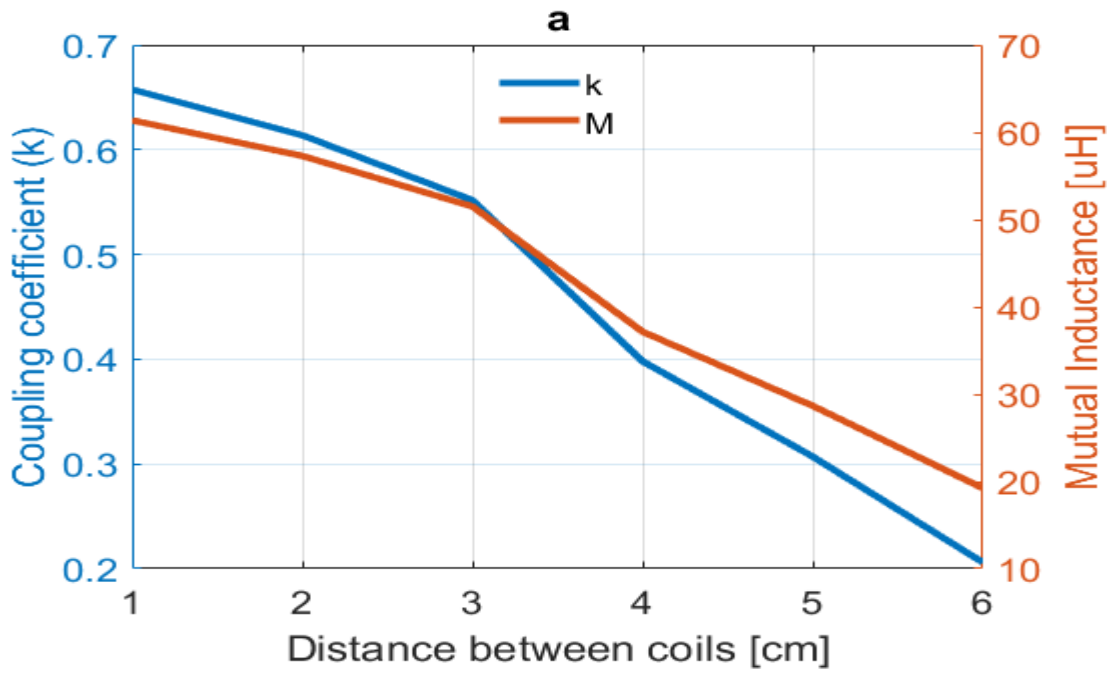

Figure 17: Mutual inductance with horizontal misalignment in air

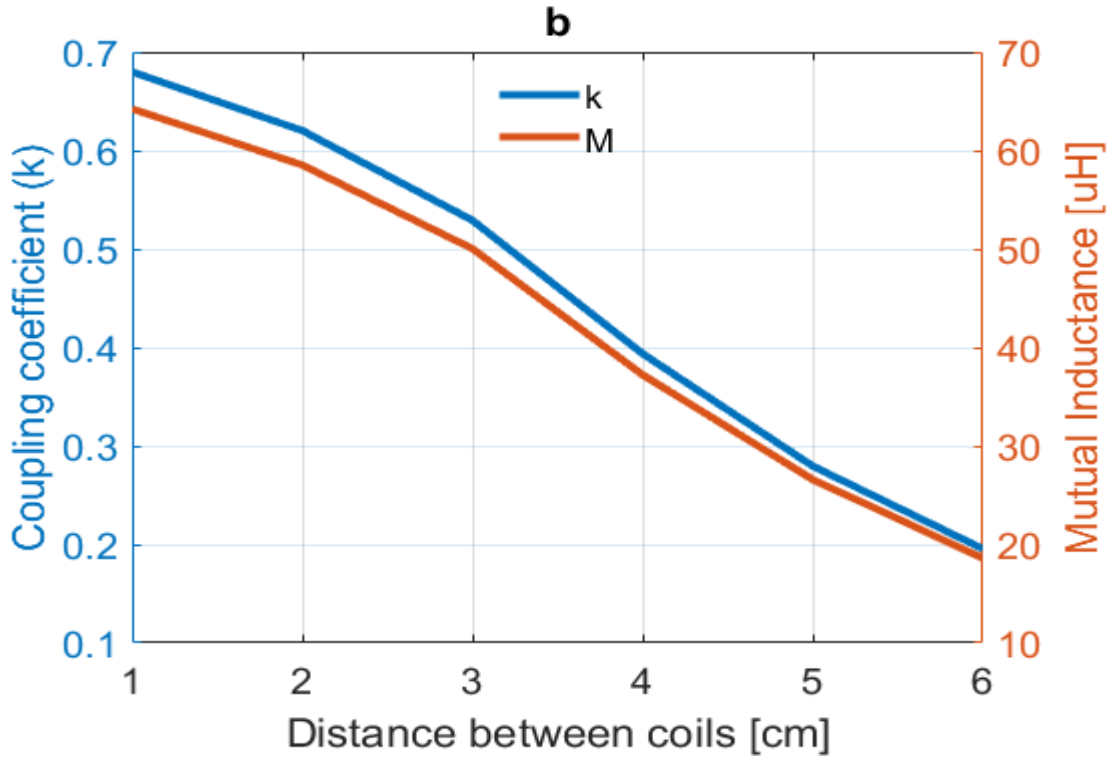

Figure 18: Mutual inductance with horizontal misalignment in water

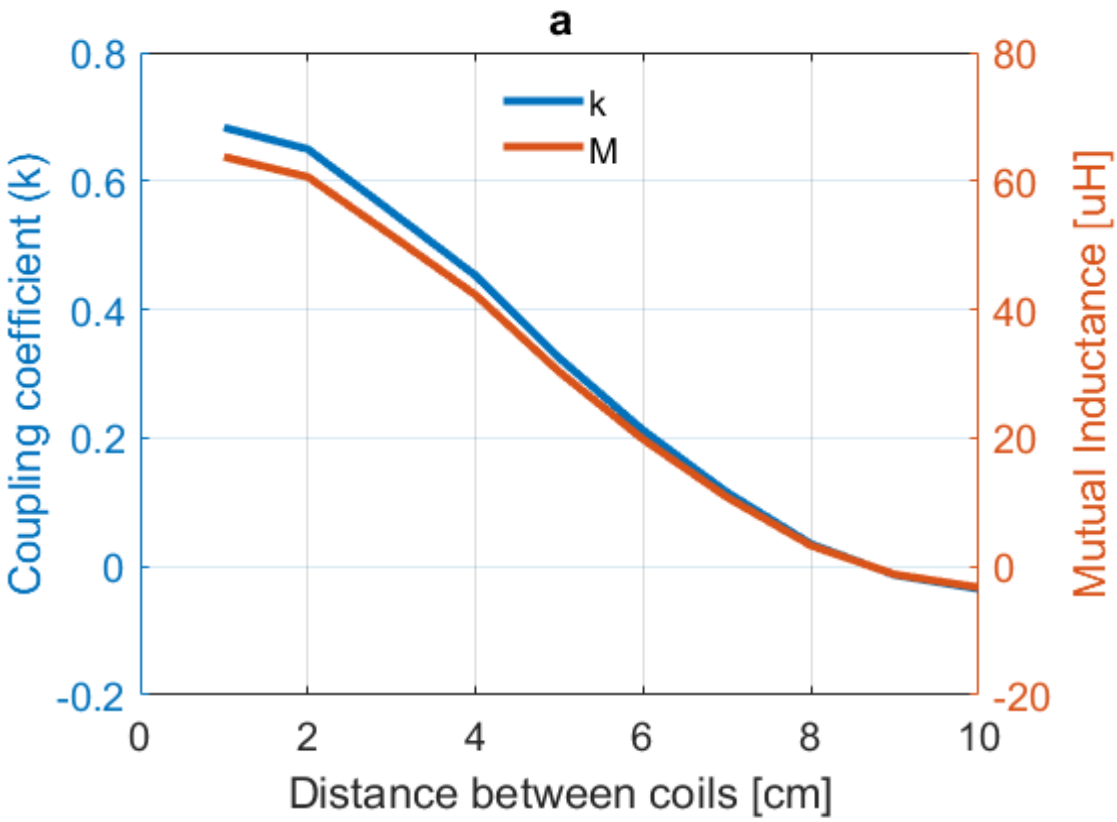

Figure 19: Mutual inductance with vertical displacement in air

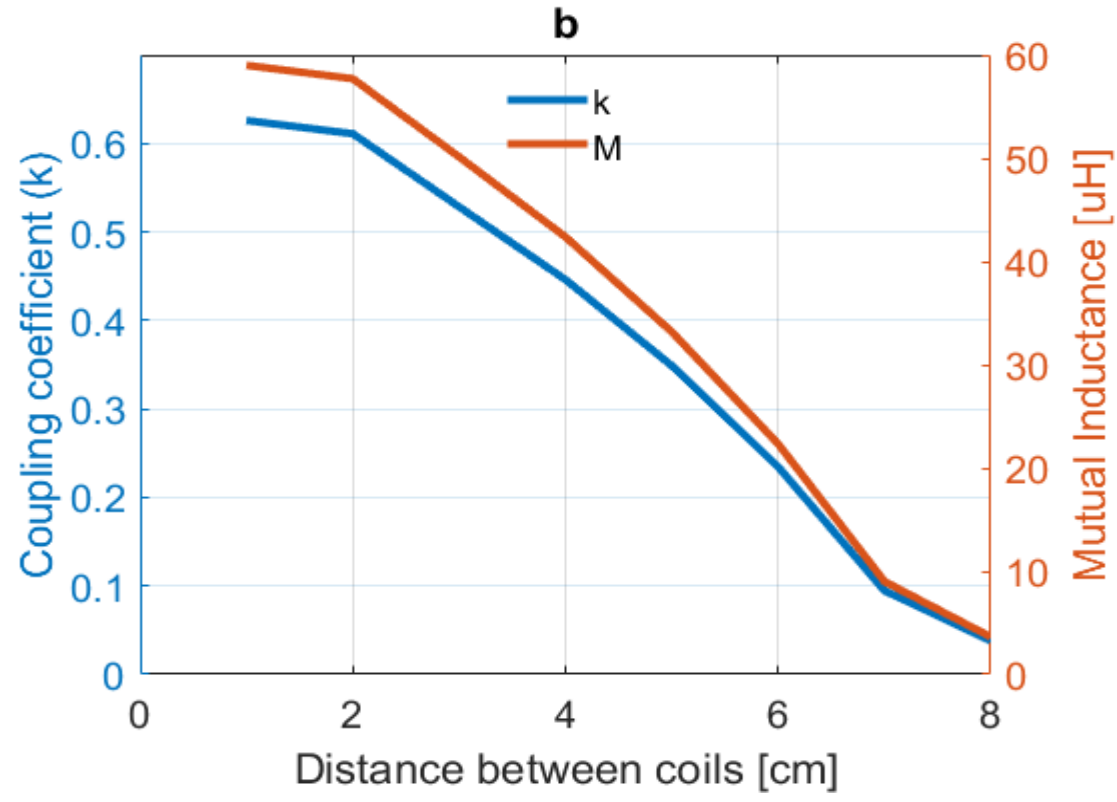

Figure 20: Mutual inductance with vertical displacement in water

The authors in [54] examine the relationship between mutual inductance and power transfer efficiency. They argue that reducing the distance between the coils does not really increase the amount of power transferred as it was conventionally believed, but there is an optimal spacing distance that will give optimal mutual inductance for maximum power transfer. They prove that the value of optimal mutual inductance for maximum power transfer is 20 µH. For our system, that means approximately 50mm distance between the coils.

According to [55], power transfer is directly proportional to the mutual inductance hence the coupling coefficient influences the transfer efficiency. A decrease in the coupling factor results in lower efficiency. Maximum efficiency is obtained with minimal distance between the coils. A plot showing the variation of the measured coil efficiency vs the coupling coefficient is shown in figure 21.

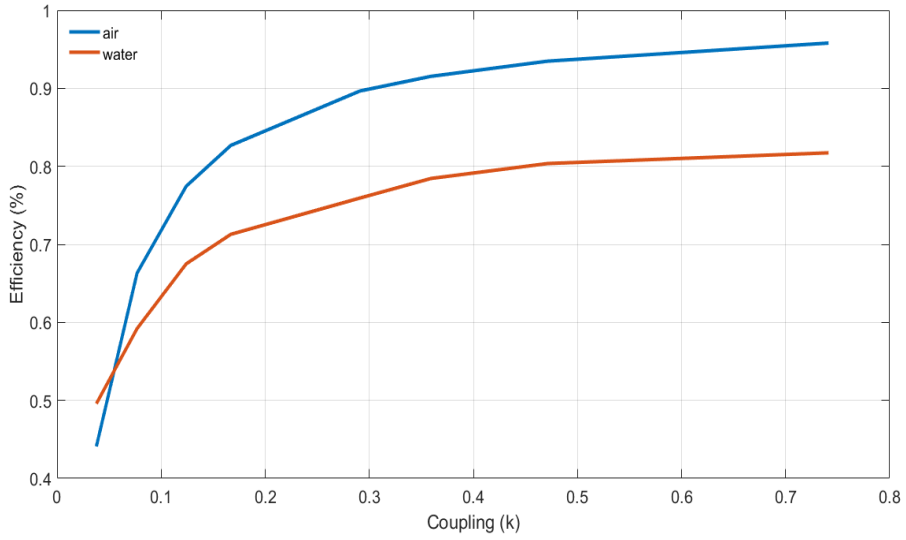

Figure 21: Variation of coil efficiency with distance

4.2.2 Converter results

The entire system was assembled and the setup prepared for testing. A picture of the test set-up can be seen on the Appendix. The input and output of the gate drive were powered using 12V dc sources. A 5V (peak to peak), 85KHz signal from a function generator was used to provide the input signal to the gate drive. The gate drive had a 2V output signal which is connected to the gate pin of the mosfet. However, this signal was too low to actually turn on the mosfet. Any attempts to increase the output power of the gate drive failed. This involved increasing the input and output voltage to the gate drive.

This could have been caused by a number of reasons such as: variation of actual component values from the simulated values, poor soldering or incorrect design of the PCB. The simulation did not account for unforeseen factors such as increase in inductance value as a result of extending the coils using cables. Some of the capacitor values used during simulation were not available and I had to use what was available in the lab. That might have caused a variation from the expected results. Due to the time limitation, I was not able to debug the circuit to understand the why the output signal from the gate drive was so low.

Chapter Summary

The circuit was designed following the design procedure described earlier in this chapter. The simulations were then done on LTspice and the graphs drawn. The coils were then made using copper wire and the inductance values measured. Thereafter, the mutual inductance and coupling coefficient were calculated. Coupling was investigated both In air and underwater and the results presented in graphs. It was noted that the mutual inductance, hence coupling coefficient, in air is higher than in water. Based on the power transfer equation (eqtn 3.25), more power is expected to be transferred in air than in water.

The two circuits were then designed on Altium and the PCBs printed in the lab. All the components were soldered and everything was ready for testing. However, the circuit did not work as expected hence no results for power transfer were obtained. The output of the gate drive was too low to turn on the mosfet. This could have been because of a number of reasons described above such as: poor soldering, incorrect design or variation of actual component values from the designed values.

CHAPTER 5: CONCLUSION AND FUTURE WORK

5.1 Conclusion

The main aim of this paper was to compare inductive coupling in air versus in water and to build a circuit to investigate power transfer across the two mediums. I was also required to design a compensation circuit for the system and to simulate the system on LTspice. I was able to achieve four out of the five required objectives.

I designed the circuit to use a class E amplifier on the transmitter side and a class E rectifier on the receiver side. I chose to implement series-series compensation because of ease of implementation. I then built the coils and did tests to determine coupling in air versus underwater and presented the results in chapter 4. I also simulated the entire system on LTspice and reported the results in chapter 4.

I built the two coils using copper wire and measured the inductance to determine self inductance and mutual inductance. I calculated the coupling coefficient based on these values. I investigated coupling both in air and in water at varying distances. I also investigated the variation of coupling with coil misalignment (horizontal and vertical) both in air and underwater. I noted that the mutual inductance and hence coupling coefficient decreases when the coils are placed underwater. The self-inductance for the coils, however increases. Mutual inductance falls almost linearly with increase in distance between the coils when placed underwater. The drop is exponential when the coils are in air. The lower mutual inductance when the coils are in water means less power gets to the receiver. This limits the distance between the boat and the charging station.

After choosing the primary and secondary coil values, I calculated the value of other circuit components. The circuit simulation was done on LTspice to investigate the behaviour of the system with regards to power output, efficiency, voltage and current. Based on the simulation analysis, I noticed that the efficiency of the class-E converter improved when the size of the inductor is reduced.

The isolated impedance inverter design is very flexible and the calculated component values can be adjusted to get more power at the output without affecting ZVS. This is desirable for UWPT because a small coil can be used to transfer more power. The electric boats are quite small hence the size of the coil should be minimized whenever possible. Also, small changes in coupling coefficient does not affect ZVS. This is important for UWPT since the coils can

easily be misaligned by waves which will change the coupling between the coils. The circuit will continue to function normally without having to change some circuit components.

5.2 Future work

Based on my experience working on this project, I would solder in the oven given another opportunity. It was quite a challenge to solder very small components using the solder gun. Some component got damaged in addition to constant short circuit on the PCB tracks due to small solder particles dropping at unintended locations. This took quite some time to rectify. Using an oven for soldering would reduce the time required for soldering by half thus saving the student a lot of time. Delivery of the components took long and this also contributed to the insufficient time available for the project. Also, if given more time, I would identify the root cause of failure for the gate drive. I needed some extra time to debug the circuit and understand why the output from the gate drive was too low.

REFERENCES

[1] R. T. O. C. O. a. Z. P. H. Feng, «Advances in High-Power Wireless Charging Systems: Overview and Design Considerations,» *IEEE Transactions on Transportation Electrification,* vol. 6, nr. 3, pp. 886-919, Sept. 2020.

[2] J. H. K. e. al., «Development of 1-MW Inductive Power Transfer System for a High-Speed Train,» *IEEE Transactions on Industrial Electronics,* vol. 62, nr. 10, pp. 6242-6250, Oct. 2015,.

[3] H. H. S. K. K. J. H. R. Z. a. J. -W. C. H. -J. Kim, «Review of Near-Field Wireless Power and Communication for Biomedical Applications,» *IEEE Access,* vol. 5, pp. 21264-21285, 2017.

[4] D. C. N. e. al., «Wireless power delivery for retinal prostheses,» *2011 Annual International Conference of the IEEE Engineering in Medicine and Biology Society,* pp. 8356-8360, 2011.

[5] B. C. a. L. M.-P. P. K. Chittoor, «A Review on UAV Wireless Charging: Fundamentals, Applications, Charging Techniques and Standards,» *IEEE Access,* vol. 9, pp. 69235-69266, 2021.

[6] C. T. a. C. M. Rim, Wireless power transfer for electric vehicles and mobile devices, John Wiley & Sons, 2017.

[7] S. J. e. al., «Design and analysis of wireless power transfer system using flexible coil and shielding material on smartwatch strap,» *2017 IEEE Wireless Power Transfer Conference (WPTC),* pp. 1-3, 2017.

[8] M. Z. C. a. R. Rahimi, «Light LED directly lit up by the wireless power transfer technology,» *2017 International Conference on Radar, Antenna, Microwave, Electronics, and Telecommunications (ICRAMET),* pp. 137-141, 2017.

[9] B. C. a. L. M.-P. A. Mahesh, «Inductive Wireless Power Transfer Charging for Electric Vehicles–A Review,» *IEEE Access,* vol. 9, pp. 137667-137713, 2021.

[10] S. J. a. A. Khan, «Design, Challenges, and Trends of Inductive Power Transfer Couplers for Electric Vehicles: A Review,» *IEEE Journal of Emerging and Selected Topics in Power Electronics,* vol. 9, nr. 5, pp. 6196-6218, Oct. 2021.

[11] K. J. a. W. Zhou, «Wireless Laser Power Transmission: A Review of Recent Progress,» *IEEE Transactions on Power Electronics,* vol. 34, nr. 4, pp. 3842-3859, April 2019.

[12] K. C. B. M. T. A. S. K. C. a. J. M. G. M. Z. Erel, «A Comprehensive Review on Wireless Capacitive Power Transfer Technology: Fundamentals and Applications,» *IEEE Access,* vol. 10, pp. 3116-3143, 2022.

[13] A. B. a. P. K. S. Deshmukh, «Comparative Analysis of Wireless Power Transmission using Microwave,» *2019 4th International Conference on Recent Trends on Electronics, Information, Communication & Technology (RTEICT),* pp. 686-690, 2019.

[14] N. Shinohara, «History and Innovation of Wireless Power Transfer via Microwaves,» *IEEE Journal of Microwaves,* vol. 1, nr. 1, pp. 218-228, Jan. 2021.

[15] D. W. N. D. M. D. a. R. D. L. B. J. Heeres, «418-423,» *Proceedings of 1994 Power Electronics Specialist Conference - PESC'94,* vol. 1, pp. 418-423, 1994.

[16] T. T. T. D. N. B. a. Z. P. C. R. Teeneti, «Review of Wireless Charging Systems for Autonomous Underwater Vehicles,» *IEEE Journal of Oceanic Engineering,* vol. 46, nr. 1, pp. 68-87, Jan. 2021.

[17] O. A. M. -S. A. a. B. S. S. Ammar, «Energy-Aware Underwater Optical System with Combined Solar Cell and SPAD Receiver,» *IEEE Communications Letters,* 2021.

[18] A. J. M. G.-G. a. J. A. A. Triviño-Cabrera, Wireless Power Transfer for Electric Vehicles: Foundations and Design Approach, Springer, 2020.

[19] C. Z. a. F. Y. K. Ye, «Dual-Hop Underwater Optical Wireless Communication System With Simultaneous Lightwave Information and Power Transfer,» *IEEE Photonics Journal,* vol. 13, nr. 6, pp. 1-77, Dec. 2021.

[20] H. K. a. G. Kaddoum, «Underwater Optical Wireless Communication,» *IEEE Access,,* vol. 4, pp. 1518-1547, 2016.

[21] B. I. L. S. H. L. G. Q. a. S. K. I. U. Khan, «Full-duplex Underwater Optical Communication Systems: A Review,» *2021 International Bhurban Conference on Applied Sciences and Technologies (IBCAST),* pp. 886-893, 2021.

[22] E. D. N. D. a. T. M. R. Guida, «Underwater Ultrasonic Wireless Power Transfer: A Battery-Less Platform for the Internet of Underwater Things,» *IEEE Transactions on Mobile Computing,* vol. 21, nr. 5, pp. 1861-1873, 1 May 2022.

[23] L. M. J. H. a. Y. F. L. Yang, «Characteristics of Undersea Capacitive Wireless Power Transfer System,» *2020 IEEE 9th International Power Electronics and Motion Control Conference (IPEMC2020-ECCE Asia),* pp. 2952-2955, 2020.

[24] M. J. a. B. Z. L. Yang, «Bidirectional Undersea Capacitive Wireless Power Transfer System,» *IEEE Access,* vol. 7, pp. 121046-121054, 2019.

[25] Y. N. K. M. a. T. N. M. Tamura, «Design of a Capacitive Wireless Power Transfer System for Operation in Fresh Water,» *IEEE Transactions on Microwave Theory and Techniques,* vol. 66, nr. 12, pp. 5873-5884, Dec. 2018.

[26] L. Y. e. al., «Analysis and design of four-plate capacitive wireless power transfer system for undersea applications,» *CES Transactions on Electrical Machines and Systems,* vol. 5, nr. 3, pp. 202-211, Sept. 2021.

[27] K. M. a. M. M. M. Tamura, «Design of Conductive Coupler for Underwater Wireless Power and Data Transfer,» *IEEE Transactions on Microwave Theory and Techniques,* vol. 69, nr. 1, pp. 1161-1175, Jan. 2021.

[28] R. M. P. P. M. a. C. C. M. T. Kan, «Design and Analysis of a Three-Phase Wireless Charging System for Lightweight Autonomous Underwater Vehicles,» *IEEE Transactions on Power Electronics,* vol. 33, nr. 8, pp. 6622-6632, Aug. 2018.

[29] Y. Z. Z. Y. P. P. M. a. C. C. M. T. Kan, «A Rotation-Resilient Wireless Charging System for Lightweight Autonomous Underwater Vehicles,» *IEEE Transactions on Vehicular Technology,* vol. 67, nr. 8, pp. 6935-6942, Aug. 2018.

[30] X. Z. Z. Z. Z. Y. B. S. a. C. C. M. K. Zhang, «A New Coil Structure to Reduce Eddy Current Loss of WPT Systems for Underwater Vehicles,» *IEEE Transactions on Vehicular Technology,* vol. 68, nr. 1, pp. 245-253, Jan. 2019.

[31] B. S. Y. Z. K. Z. Z. M. a. Y. H. Z. Yan, «A Rotation-Free Wireless Power Transfer System With Stable Output Power and Efficiency for Autonomous Underwater Vehicles,» *IEEE Transactions on Power Electronics,* vol. 34, nr. 5, pp. 4005-4008, May 2019.

[32] K. Z. L. Q. Y. H. a. B. S. Z. Yan, «A Multi-Load Wireless Power Transfer System with Concentrated Magnetic Field for AUV Cluster System,» *IEEE Transactions on Industry Applications,* 2021.

[33] Y. Z. S. W. J. L. Z. Z. a. L. J. C. Cai, «A Circumferential Coupled Dipole-Coil Magnetic Coupler for Autonomous Underwater Vehicles Wireless Charging Applications,» *IEEE Access,* vol. 8, pp. 65432-65442, 2020.

[34] S. C. J. Z. Z. B. K. S. a. C. Z. D. Wang, «A Novel Arc-Shaped Lightweight Magnetic Coupler for AUV Wireless Power Transfer,» *IEEE Transactions on Industry Applications,* 2021.

[35] Y. Z. e. al., «Misalignment Insensitive Wireless Power Transfer System Using a Hybrid Transmitter for Autonomous Underwater Vehicles,» *IEEE Transactions on Industry Applications,* 2021.

[36] P. Y. Y. C. K. G. S. H. a. H. S. J. Zhou, «Design Considerations for a Self-Latching Coupling Structure of Inductive Power Transfer for Autonomous Underwater Vehicle,» *IEEE Transactions on Industry Applications,* vol. 57, nr. 1, pp. 580-587, Jan.-Feb. 2021.

[37] K. O. S. K. K. E. a. Y. K. R. Hasaba, «Magnetic Resonance Wireless Power Transfer Over 10 m With Multiple Coils Immersed in Seawater,» *IEEE Transactions on Microwave Theory and Techniques,* vol. 67, nr. 11, pp. 4505-4513, Nov. 2019.

[38] G. A. C. a. O. H. S. Chwei-Sen Wang, «Power transfer capability and bifurcation phenomena of loosely coupled inductive power transfer systems,» *IEEE Transactions on Industrial Electronics,* vol. 51, nr. 1, pp. 148-157, Feb. 2004.

[39] O. H. R. S. B. P. N. P. a. N. S. V. Shevchenko, «Compensation Topologies in IPT Systems: Standards, Requirements, Classification, Analysis, Comparison and Application,» *IEEE Access,* vol. 7, pp. 120559-120580, 2019.

[40] G. A. C. a. O. H. S. Chwei-Sen Wang, «Power transfer capability and bifurcation phenomena of loosely coupled inductive power transfer systems,» *IEEE Transactions on Industrial Electronics,* vol. 51, nr. 1, pp. 148-157, Feb. 2004.

[41] Z. Y. e. al., «Frequency Optimization of a Loosely Coupled Underwater Wireless Power Transfer System Considering Eddy Current Loss,» *IEEE Transactions on Industrial Electronics,* vol. 66, nr. 5, pp. 3468-3476, May 2019.

[42] K. K. H. K. D. K. J. P. a. S. A. J. Kim, «An Efficient Modeling for Underwater Wireless Power Transfer Using Z-Parameters,» *IEEE Transactions on Electromagnetic Compatibility,* vol. 61, nr. 6, pp. 2006-2014, Dec. 2019.

[43] Y. M. Z. Y. Z. D. B. S. a. A. P. H. K. Zhang, «Eddy Current Loss and Detuning Effect of Seawater on Wireless Power Transfer,» *IEEE Journal of Emerging and Selected Topics in Power Electronics,* vol. 8, nr. 1, pp. 909-917, March 2020.

[44] R. A. C. R. T. a. J. L. Z. N. Low, «Design and Test of a High-Power High-Efficiency Loosely Coupled Planar Wireless Power Transfer System,» *IEEE Transactions on Industrial Electronics,* vol. 56, nr. 5, pp. 1801-1812, May 2009.

[45] G. A. K. e. al., «An optimal design methodology for inductive power link with class-E amplifier,» *IEEE Transactions on Circuits and Systems I: Regular Papers,* vol. 52, nr. 5, pp. 857-866, May 2005.

[46] N. O. S. a. A. D. Sokal, «Class E-A new class of high-efficiency tuned single-ended switching power amplifiers,» *IEEE Journal of Solid-State Circuits,* vol. 10, nr. 3, pp. 168-176, June 1975.

[47] X. W. E. B. E. A. M. K. K. a. H. S. T. Nagashima, «Steady-State Analysis of Isolated Class-E^2 Converter Outside Nominal Operation,» *IEEE Transactions on Industrial Electronics,* vol. 64, nr. 4, pp. 3227-3238, April 2017.

[48] M. K. Kazimierczuk, «Class E Zero-Voltage Switching RF Power,» i *RF power amplifiers*, John Wiley & Sons, 2014, pp. 243- 305.

[49] M. K. Kazimierczuk, «Transformers,» i *High-frequency magnetic components*, John Wiley & Sons, 2009, pp. 412-471.

[50] M. K. Kazimierczuk, High-frequency magnetic components, John Wiley & Sons, 2009.

[51] F. G. A. R. A. A. D. K. S. a. M. K. K. F. Corti, «Design of class-E ZVS inverter with loosely-coupled transformer at fixed coupling coefficient,» i *IECON 2016- 42nd Annual Conference of the IEEE Industrial Electronics Society*, Florence, Italy, 2016.

[52] A. &. F. M. J. Grebennikov, Switchmode RF and microwave power amplifiers, Academic Press, 2021.

[53] L. G. Z. Y. K. S. a. J. R.-D. Z. Tong, «On the Techniques to Utilize SiC Power Devices in High- and Very High-Frequency Power Converters,» *IEEE Transactions on Power Electronics,* vol. 34, nr. 12, pp. 12181-12192, Dec. 2019.

[54] P. W. Z. H. Y. -S. S. S. R. a. J. .. -C. C. M. Q. Nguyen, «A mutual inductance approach for optimization of wireless energy transmission,» *Texas Symposium on Wireless and Microwave Circuits and Systems,* pp. 1-4, 2014.

[55] Z. L. a. J. W. H. Wen, «Effects of coil parameters on transfer efficiency in LCL wireless power transfer system,» *2017 IEEE PELS Workshop on Emerging Technologies: Wireless Power Transfer (WoW),* pp. 1-5, 2017.

[56] C. A. a. P. Intani, «Wireless Power Transfer for Autonomous Underwater Vehicle,» *2020 IEEE PELS Workshop on Emerging Technologies: Wireless Power Transfer (WoW),* pp. 246-249, 2020.

[57] M. S.-A. a. N. C. K. B. Esteban, «A Comparative Study of Power Supply Architectures in Wireless EV Charging Systems,» *IEEE Transactions on Power Electronics,* vol. 30, nr. 11, pp. 6408-6422, Nov. 2015.

[58] B. C. a. L. M.-P. A. Mahesh, «Inductive Wireless Power Transfer Charging for Electric Vehicles–A Review,» *IEEE Access,* vol. 9, pp. 137667-137713,, 2021.

[59] P. W. Z. H. Y. -S. S. S. R. a. J. .. -C. C. M. Q. Nguyen, «A mutual inductance approach for optimization of wireless energy transmission,» *Texas Symposium on Wireless and Microwave Circuits and Systems,* pp. 1-4, 2014.

[60] S. J. e. al., «Smartwatch Strap Wireless Power Transfer System With Flexible PCB Coil and Shielding Material,» *IEEE Transactions on Industrial Electronics,* vol. 66, nr. 5, pp. 4054-4064, May 2019.

[61] M. H. a. A. E. Zawawi, «Wireless power transfer (Wireless lighting),» *2015 5th International Conference on Information & Communication Technology and Accessibility (ICTA),* pp. 1-4, 2015.

APPENDIX

Assembly Drawings

Receiver Top

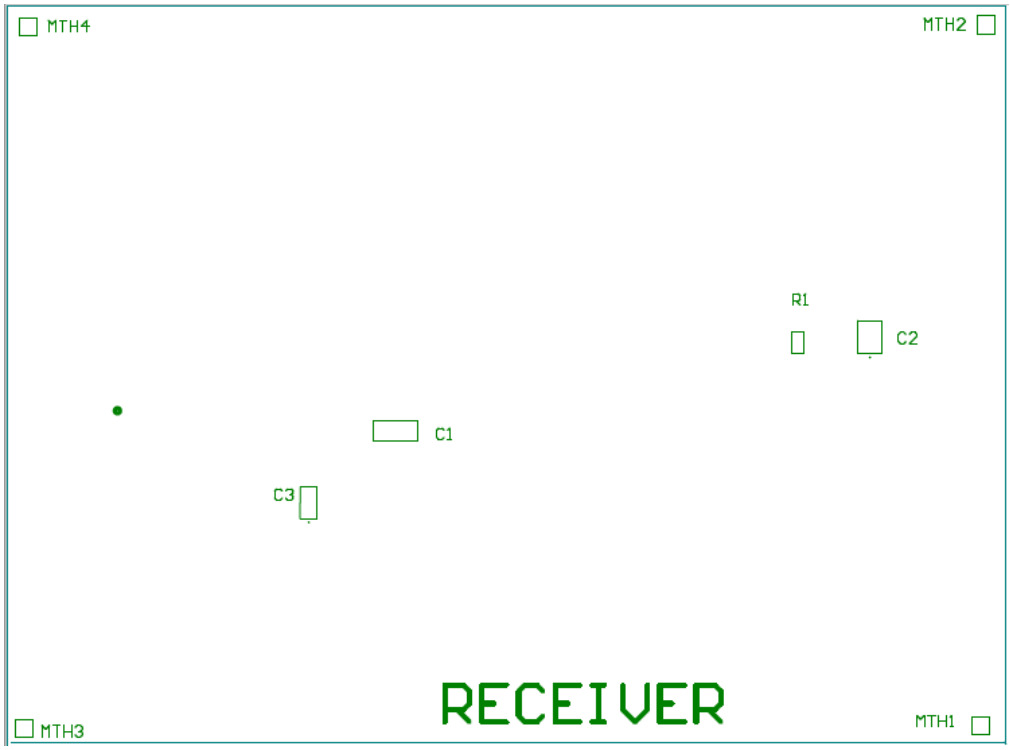

Receiver Bottom

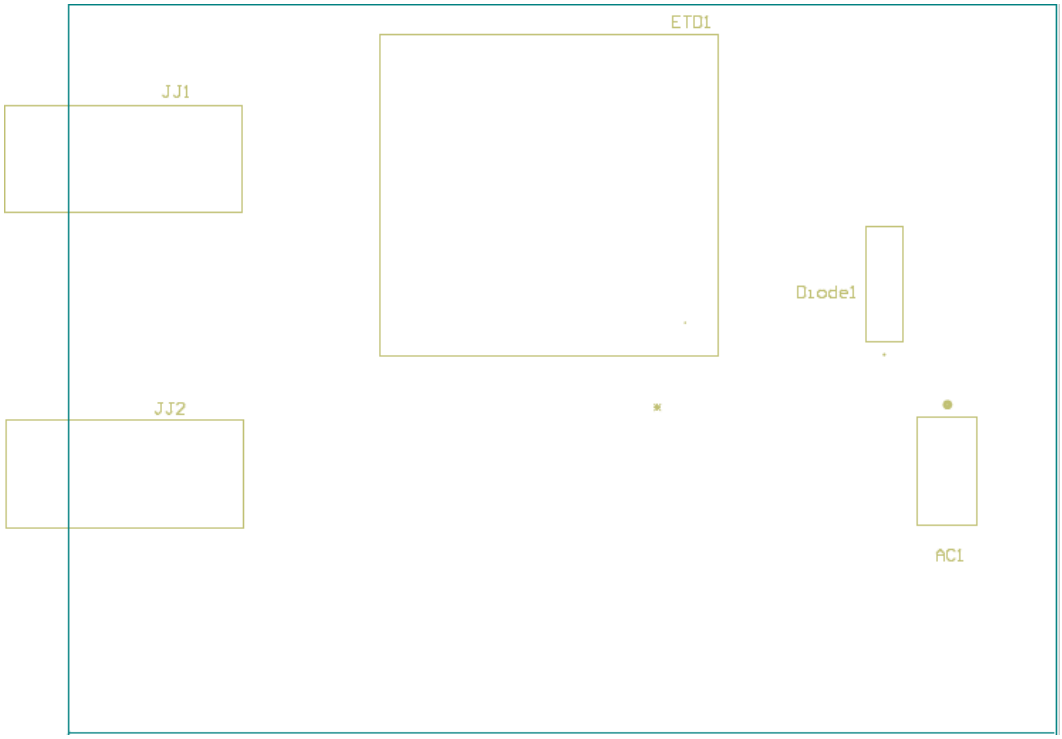

TRANSMITTER TOP

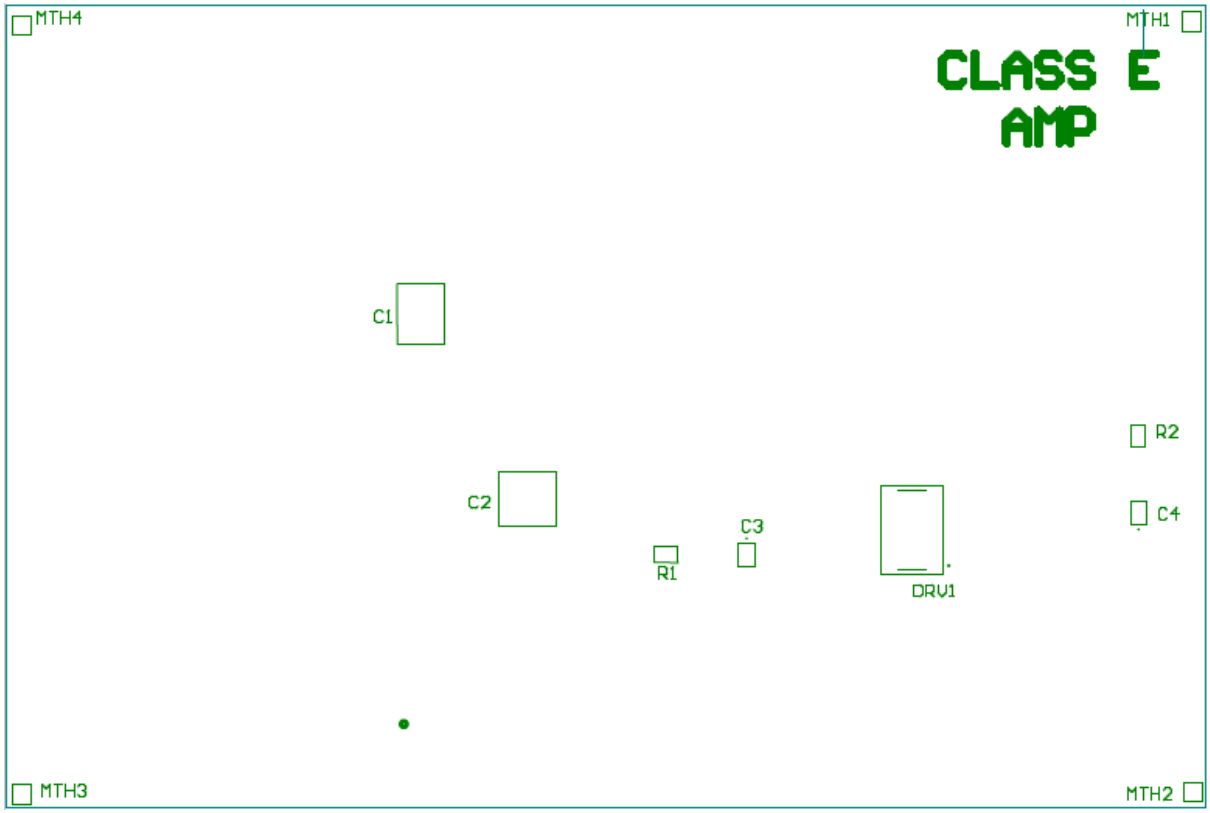

TRANSMITTER BOTTOM

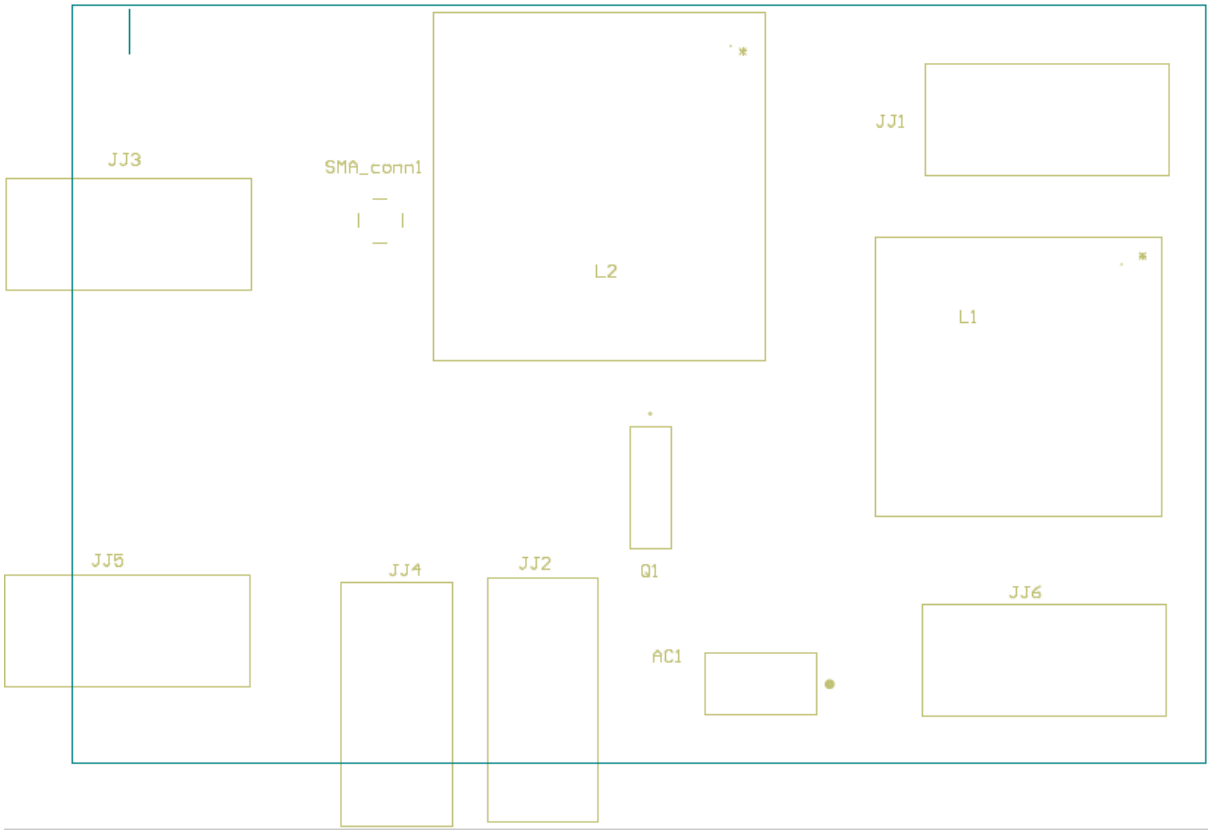

Coils

Figure 22: Actual transmitter and receiver coil

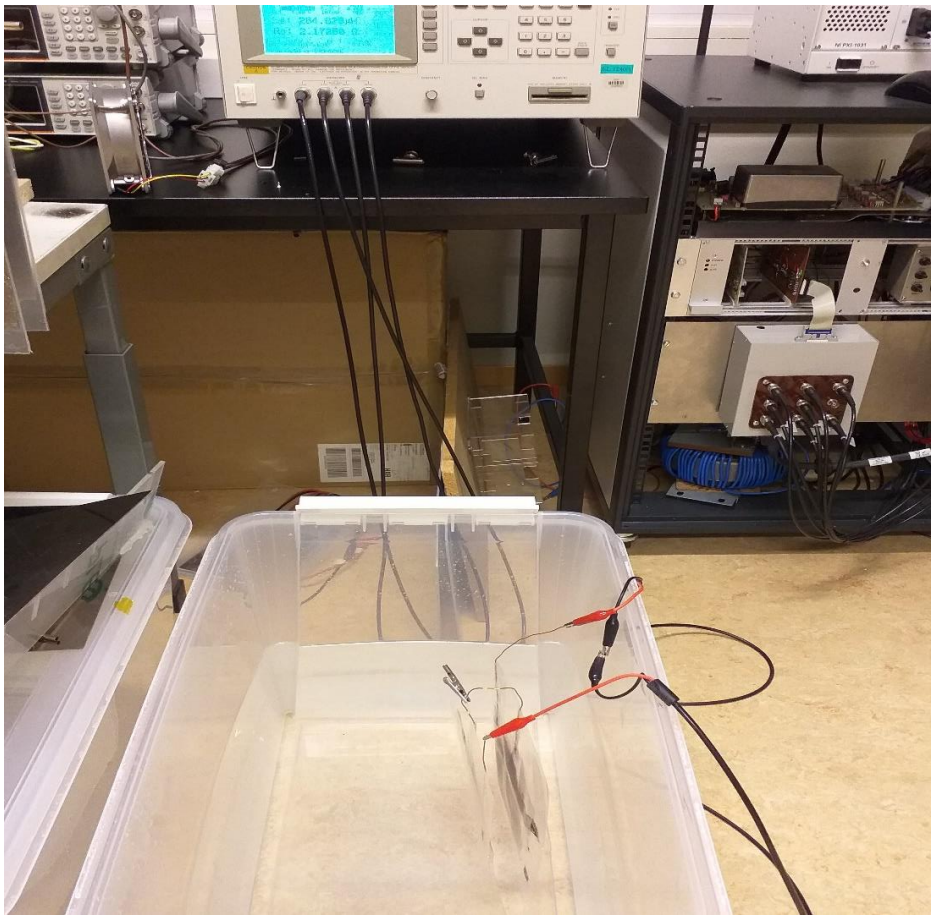

Figure 23: Test set-up

PCB

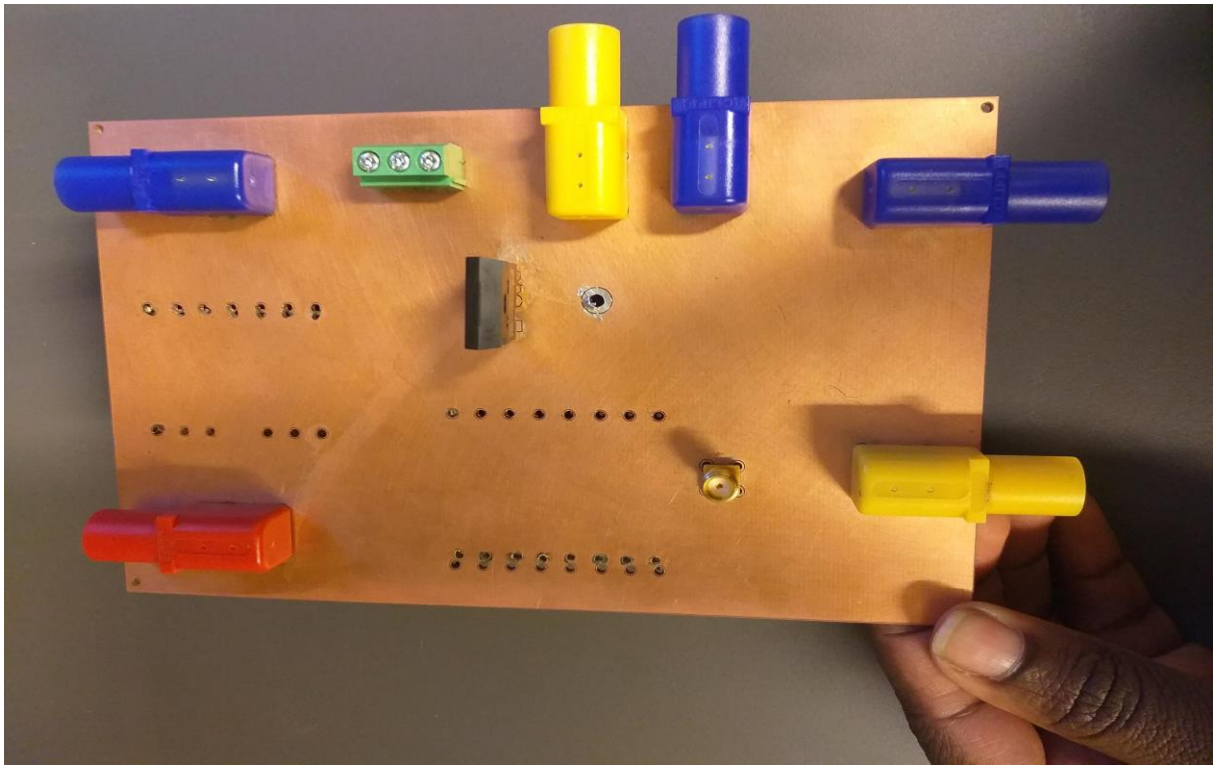

Figure 24: Transmitter bottom side

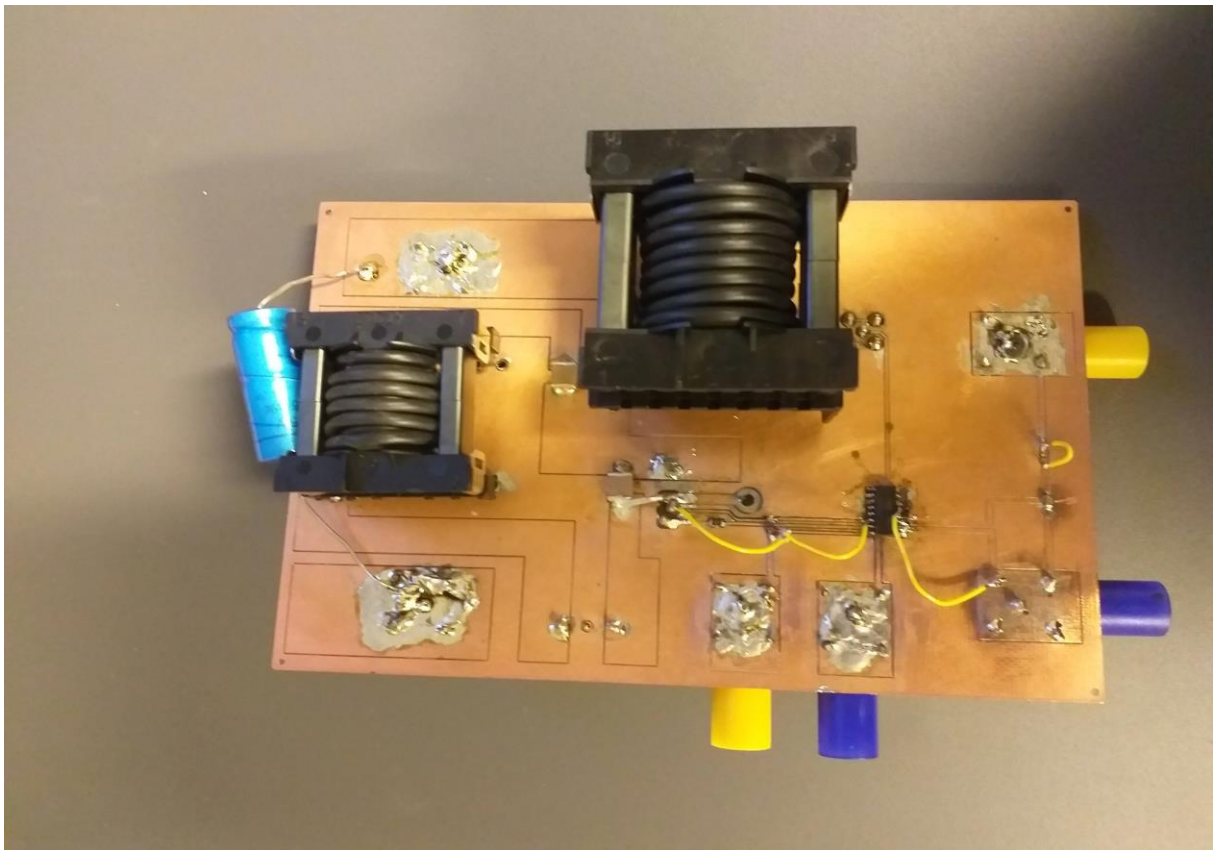

Figure 25: Transmitter top side

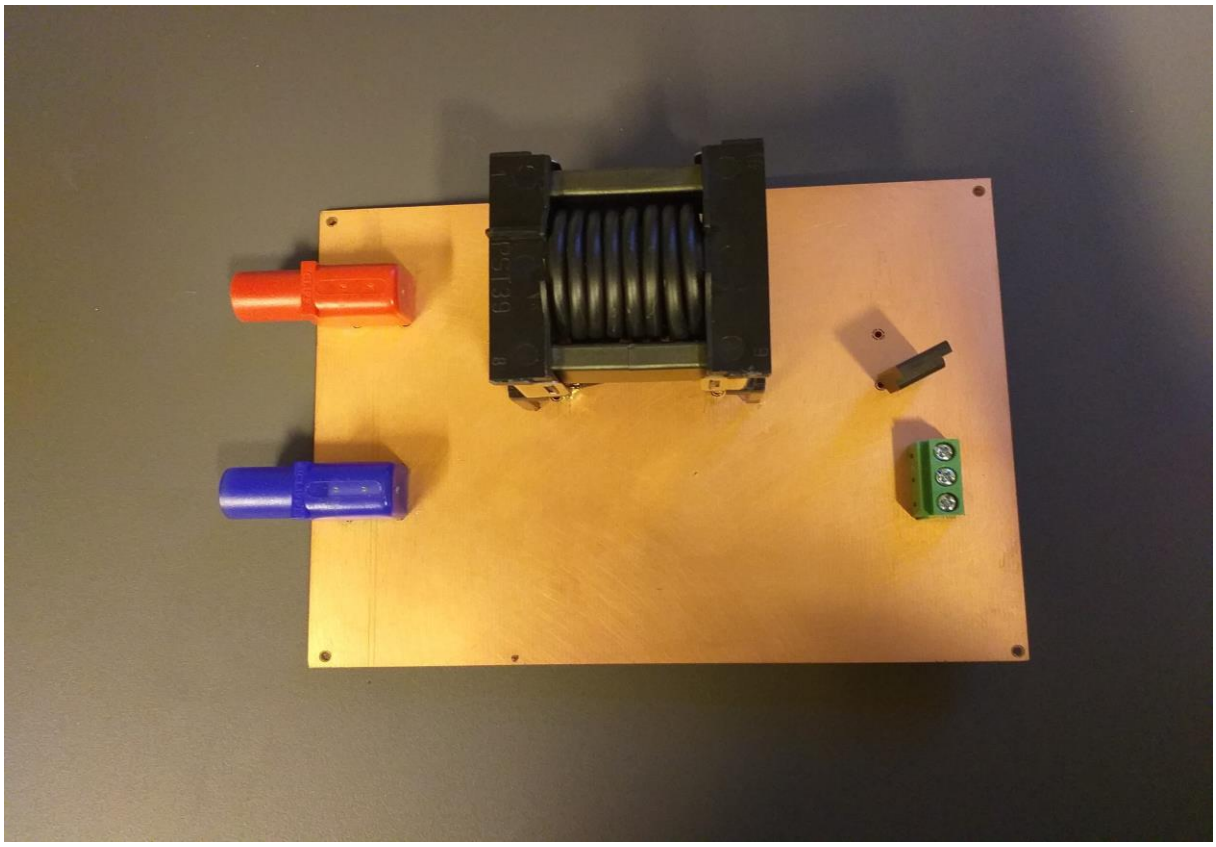

Figure 26: Receiver bottom side

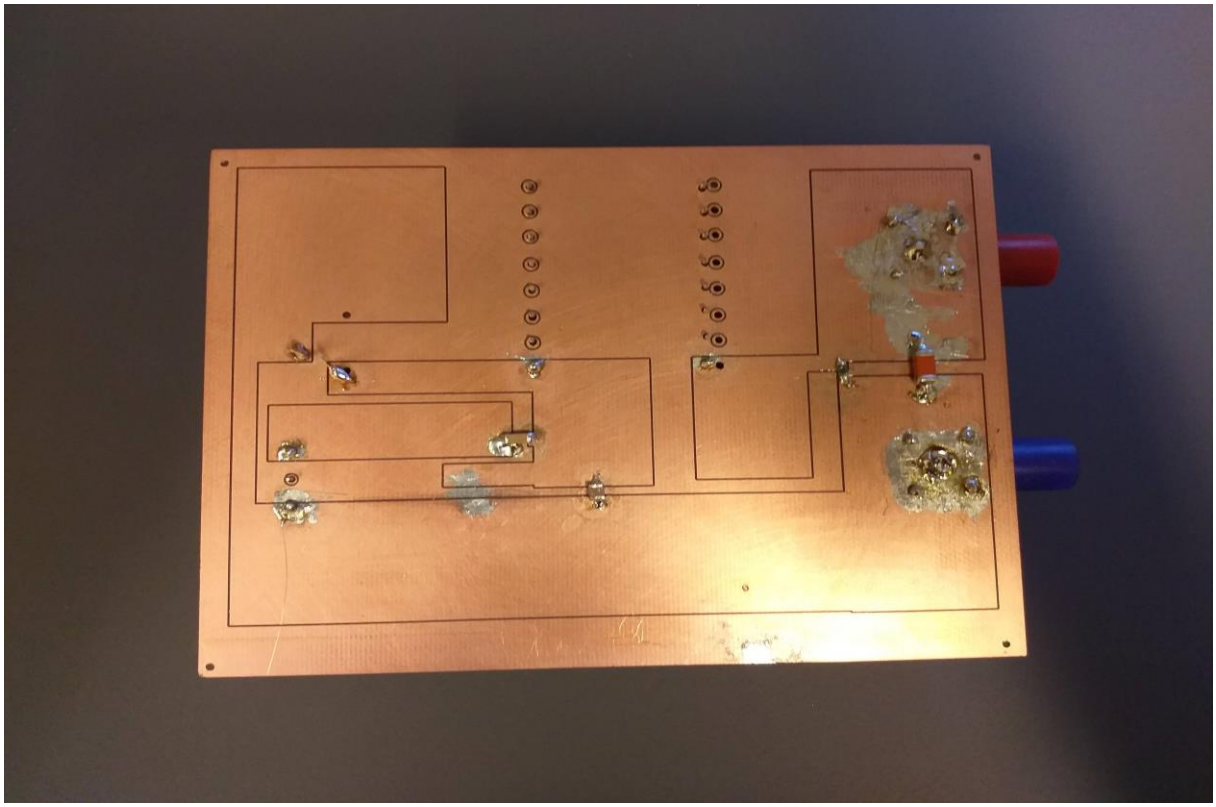

Figure 27: Receiver top side

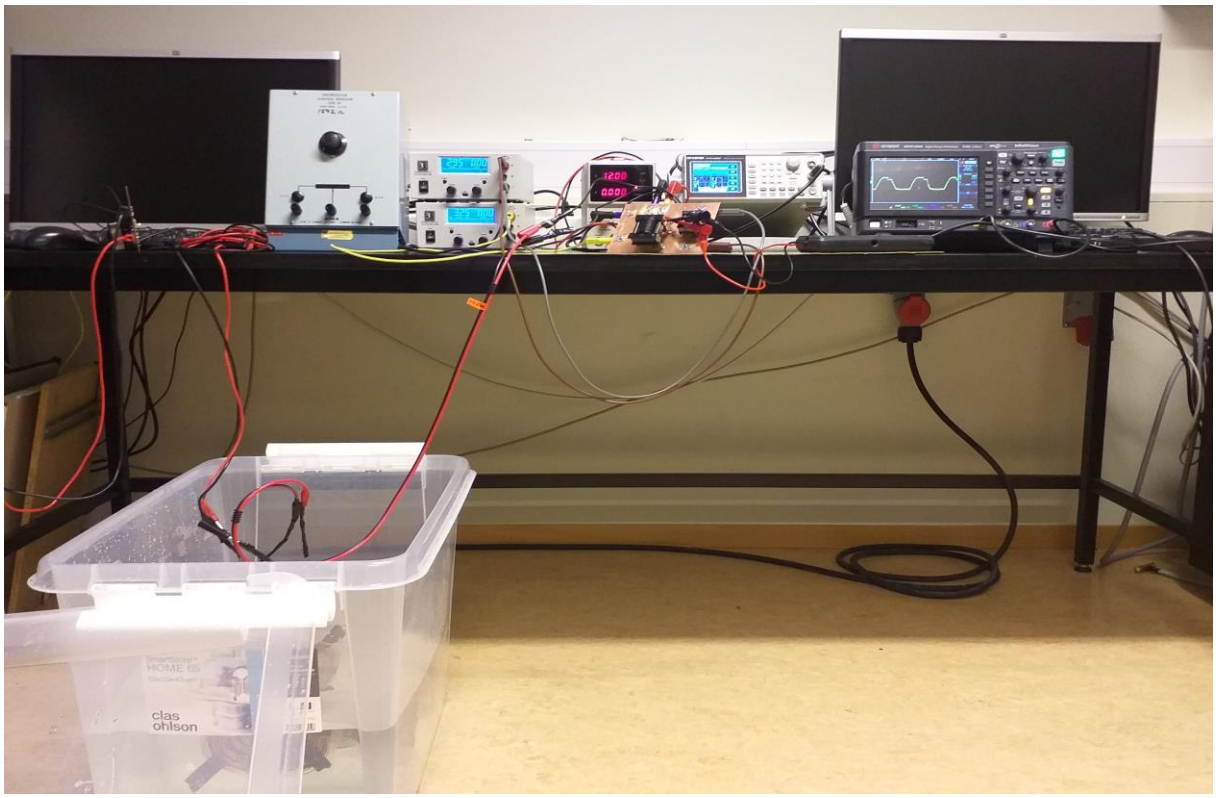

Figure 28: Final setup

MATLAB Script

```
Lp= 140*(10^-6);
Ls= 105*(10^-6);

Vin= 60;
Po= 300;
fs= 85000;
w= 2*pi*fs;
QL=7;
k=0.3;
n= Lp/Ls;

Rir= 0.5768*((Vin^2)/Po);
Ri= (n^2)*Rir;

%equivalent input resistance
Rti= ((w^2)*(Lp^2)*(k^2)*Ri)/((Ri^2)+((w^2)*(k^2)*(Lp^2)));

%equivalent input inductance
Lti=((w^2)*(Lp^3)*(k^2)*(1-k)+(Lp*(Ri^2)))/((Ri^2)+((w^2)*(k^2)*(Lp^2)));

%magnetizing inductace
Lm= Ri/(w*sqrt((Ri/Rti)-1));

%primary and secondary leakage inductance
Llp= (1-k)*Lp;
Lls= (1-k)*Lp;

%secondary side resonant tank capacitance required to nullify leakage indcutance
Cs= (n^2)/(4*(pi^2)*(fs^2)*(1-k)*Lp);

%Inductance
Li= (Rti/w)*(QL- sqrt((Ri/Rti)-1));

Lext= Li-Llp;

%Total inductance in resonant circuit, L
L= Lext + Lti;

%Resonant capacitor in series with L
C= 1/(w*(QL-((pi^3)-(4*pi))/16)*Rti);

%Choke inductance Lf
Lf= 6.934802201*(Rti/(4*fs));

%Shunt capacitor
C1= 8/(w*pi*((pi^2)+4)*Rti);

Co=56*(10^-12);
C1ext=C1-Co;
```